

The WiggleZ Dark Energy Survey: mapping the distance–redshift relation with baryon acoustic oscillations

Chris Blake,^{1*} Eyal A. Kazin,² Florian Beutler,³ Tamara M. Davis,^{4,5}
David Parkinson,⁴ Sarah Brough,⁶ Matthew Colless,⁶ Carlos Contreras,¹
Warrick Couch,¹ Scott Croom,⁷ Darren Croton,¹ Michael J. Drinkwater,⁴ Karl Forster,⁸
David Gilbank,⁹ Mike Gladders,¹⁰ Karl Glazebrook,¹ Ben Jelliffe,⁷ Russell J. Jurek,¹¹
I-hui Li,¹ Barry Madore,¹² D. Christopher Martin,⁸ Kevin Pimbblet,¹³
Gregory B. Poole,¹ Michael Pracy,^{1,14} Rob Sharp,^{6,14} Emily Wisnioski,¹
David Woods,¹⁵ Ted K. Wyder⁸ and H. K. C. Yee¹⁶

¹Centre for Astrophysics & Supercomputing, Swinburne University of Technology, PO Box 218, Hawthorn, VIC 3122, Australia

²Center for Cosmology and Particle Physics, New York University, 4 Washington Place, New York, NY 10003, USA

³International Centre for Radio Astronomy Research, University of Western Australia, 35 Stirling Highway, Perth WA 6009, Australia

⁴School of Mathematics and Physics, University of Queensland, Brisbane, QLD 4072, Australia

⁵Dark Cosmology Centre, Niels Bohr Institute, University of Copenhagen, Juliane Maries Vej 30, DK-2100 Copenhagen Ø, Denmark

⁶Australian Astronomical Observatory, PO Box 296, Epping, NSW 1710, Australia

⁷Sydney Institute for Astronomy, School of Physics, University of Sydney, NSW 2006, Australia

⁸California Institute of Technology, MC 278-17, 1200 East California Boulevard, Pasadena, CA 91125, USA

⁹Astrophysics and Gravitation Group, Department of Physics and Astronomy, University of Waterloo, Waterloo, ON N2L 3G1, Canada

¹⁰Department of Astronomy and Astrophysics, University of Chicago, 5640 South Ellis Avenue, Chicago, IL 60637, USA

¹¹Australia Telescope National Facility, CSIRO, Epping, NSW 1710, Australia

¹²Observatories of the Carnegie Institute of Washington, 813 Santa Barbara St., Pasadena, CA 91101, USA

¹³School of Physics, Monash University, Clayton, VIC 3800, Australia

¹⁴Research School of Astronomy & Astrophysics, Australian National University, Weston Creek, ACT 2611, Australia

¹⁵Department of Physics & Astronomy, University of British Columbia, 6224 Agricultural Road, Vancouver, BC V6T 1Z1, Canada

¹⁶Department of Astronomy and Astrophysics, University of Toronto, 50 St. George Street, Toronto, ON M5S 3H4, Canada

Accepted 2011 August 5. Received 2011 August 4; in original form 2011 July 1

ABSTRACT

We present measurements of the baryon acoustic peak at redshifts $z = 0.44, 0.6$ and 0.73 in the galaxy correlation function of the final data set of the WiggleZ Dark Energy Survey. We combine our correlation function with lower redshift measurements from the 6-degree Field Galaxy Survey and Sloan Digital Sky Survey, producing a stacked survey correlation function in which the statistical significance of the detection of the baryon acoustic peak is 4.9σ relative to a zero-baryon model with no peak. We fit cosmological models to this combined baryon acoustic oscillation (BAO) data set comprising six distance–redshift data points, and compare the results with similar cosmological fits to the latest compilation of supernovae (SNe) and cosmic microwave background (CMB) data. The BAO and SNe data sets produce consistent measurements of the equation-of-state w of dark energy, when separately combined with the CMB, providing a powerful check for systematic errors in either of these distance probes. Combining all data sets we determine $w = -1.03 \pm 0.08$ for a flat universe, consistent with a cosmological constant model. Assuming dark energy is a cosmological constant and varying the spatial curvature, we find $\Omega_k = -0.004 \pm 0.006$.

Key words: surveys – cosmological parameters – distance scale – large-scale structure of Universe.

*E-mail: cblake@astro.swin.edu.au

1 INTRODUCTION

Measurements of the cosmic distance–redshift relation have always constituted one of the most important probes of the cosmological model. 80 years ago such observations provided evidence that the Universe is expanding; more recently they have convincingly suggested that this expansion rate is accelerating. The distance–redshift relation depends on the expansion history of the Universe, which is in turn governed by its physical contents including the properties of the ‘dark energy’ which has been hypothesized to be driving the accelerating expansion. One of the most important challenges in contemporary cosmology is to distinguish between the different possible physical models for dark energy, which include a material or scalar field smoothly filling the Universe with a negative equation of state, a modification to the laws of gravity at large cosmic scales or the effects of inhomogeneity on cosmological observations. Cosmological distance measurements provide one of the crucial observational data sets to help distinguish between these different models.

One of the most powerful tools for mapping the distance–redshift relation is Type Ia supernovae (SNe Ia). About a decade ago, observations of nearby and distant SNe Ia provided some of the most compelling evidence that the expansion rate of the Universe is accelerating (Riess et al. 1998; Perlmutter et al. 1999), in agreement with earlier suggestions based on comparisons of the cosmic microwave background (CMB) and large-scale structure data (Efstathiou, Sutherland & Maddox 1990; Krauss & Turner 1995; Ostriker & Steinhardt 1995). Since then, the sample of SNe Ia available for the cosmological analysis has grown impressively due to a series of large observational projects which has populated the Hubble diagram across a range of redshifts. These projects include the Nearby Supernova Factory (Copin et al. 2006), the Center for Astrophysics SN group (Hicken et al. 2009), the Carnegie Supernova Project (Hamuy et al. 2006) and the Palomar Transient Factory (Law et al. 2009) at low redshifts $z < 0.1$; the Sloan Digital Sky Survey (SDSS) supernova survey (Kessler et al. 2009) at low-to-intermediate redshifts $0.1 < z < 0.3$; the Supernova Legacy Survey (Astier et al. 2006) and ESSENCE (Wood-Vasey et al. 2007) projects at intermediate redshifts $0.3 < z < 1.0$; and observations by the *Hubble Space Telescope* at high redshifts $z > 1$ (Riess et al. 2004, 2007; Dawson et al. 2009). These supernovae (SNe) data have been collected and analysed in a homogeneous fashion in the ‘Union’ SNe compilations, initially by Kowalski et al. (2008) and most recently by Amanullah et al. (2010) in the ‘Union 2’ sample of 557 SNe Ia.

The utility of these SNe data sets is now limited by known (and potentially unknown) systematic errors which could bias cosmological fits if not handled correctly. These systematics include redshift-dependent astrophysical effects, such as potential drifts with redshift in the relations between colour, luminosity and light-curve shape owing to evolving SNe Ia populations, and systematics in the analysis such as the fitting of light curves, photometric zero-points, K -corrections and the Malmquist bias. Although these systematics have been treated very thoroughly in recent SNe analyses, it is clearly desirable to cross-check the cosmological conclusions with other probes of the distance–redshift relation.

A very promising and complementary method for mapping the distance–redshift relation is the measurement of baryon acoustic oscillations (BAOs) in the large-scale clustering pattern of galaxies, and their application as a cosmological standard ruler (Eisenstein, Hu & Tegmark 1998; Cooray et al. 2001; Blake & Glazebrook 2003;

Eisenstein 2003; Hu & Haiman 2003; Linder 2003; Seo & Eisenstein 2003). BAOs correspond to a preferred length-scale imprinted in the distribution of photons and baryons by the propagation of sound waves in the relativistic plasma of the early Universe (Peebles & Yu 1970; Sunyaev & Zeldovitch 1970; Bond & Efstathiou 1984; Holtzman 1989; Hu & Sugiyama 1996; Eisenstein & Hu 1998). This length-scale, which corresponds to the sound horizon at the baryon drag epoch denoted by $r_s(z_d)$, may be predicted very accurately by measurements of the CMB which yield the physical matter and baryon densities that control the sound speed, expansion rate and recombination time in the early Universe: the latest determination is $r_s(z_d) = 153.3 \pm 2.0$ Mpc (Komatsu et al. 2009). In the pattern of late-time galaxy clustering, BAOs manifest themselves as a small preference for pairs of galaxies to be separated by $r_s(z_d)$, causing a distinctive ‘baryon acoustic peak’ to be imprinted in the two-point galaxy correlation function. The corresponding signature in the Fourier space is a series of decaying oscillations or ‘wiggles’ in the galaxy power spectrum.

Measurement of BAOs has become an important motivation for galaxy redshift surveys in recent years. The small amplitude of the baryon acoustic peak, and the large size of the relevant scales, implies that cosmic volumes of the order of 1 Gpc^3 must be mapped with of the order of 10^5 galaxies to ensure a robust detection (Tegmark 1997; Blake & Glazebrook 2003; Glazebrook & Blake 2005; Blake et al. 2006). Significant detections of BAOs have now been reported by three independent galaxy surveys, spanning a range of redshifts $z \leq 0.6$: the SDSS, the WiggleZ Dark Energy Survey and the 6-degree Field Galaxy Survey (6dFGS).

The most accurate BAO measurements have been obtained by analysing the SDSS, particularly the Luminous Red Galaxy (LRG) component. Eisenstein et al. (2005) reported a convincing detection of the acoustic peak in the two-point correlation function of the SDSS Third Data Release (DR3) LRG sample with effective redshift $z = 0.35$. Percival et al. (2010) performed a power spectrum analysis of the SDSS DR7 data set, considering both the main and LRG samples, and measured the distance–redshift relation at both $z = 0.2$ and $z = 0.35$ with ~ 3 per cent accuracy in units of the standard ruler scale. Other studies of the SDSS-LRG sample, producing broadly similar conclusions, have been undertaken by Hutsi (2006), Percival et al. (2007), Sánchez et al. (2009) and Kazin et al. (2010a). These studies of SDSS galaxy samples built on hints of BAOs reported by the 2-degree Field Galaxy Redshift Survey (Percival et al. 2001; Cole et al. 2005) and combinations of smaller data sets (Miller, Nichol & Batuski 2001). There have also been potential BAO detections in photometric-redshift catalogues from the SDSS (Blake et al. 2007; Padmanabhan et al. 2007; Crocce et al. 2011), although the statistical significance of these measurements currently remains much lower than that which can be obtained using spectroscopic redshift catalogues.

These BAO detections have recently been supplemented by new measurements from two different surveys, which have extended the redshift coverage of the standard ruler technique. In the low-redshift Universe the 6dFGS has reported a BAO detection at $z = 0.1$ (Beutler et al. 2011). This study produced an ~ 5 per cent measurement of the standard ruler scale and a new determination of the Hubble constant H_0 . At higher redshifts the WiggleZ Survey has quantified BAOs at $z = 0.6$, producing an ~ 4 per cent measurement of the baryon acoustic scale (Blake et al. 2011). Taken together, these different galaxy surveys have demonstrated that BAO standard ruler measurements are self-consistent with the standard cosmological model established from CMB observations, and have yielded new, tighter constraints on cosmological parameters.

The accuracy with which BAOs may be used to determine the distance–redshift relation using current surveys is limited by statistical rather than systematic errors (in contrast to observations of SNe Ia). The measurement error in the large-scale correlation function, which governs how accurately the preferred scale may be extracted, is determined by the volume of the large-scale structure mapped and the number density and bias of the galaxy tracers. There are indeed potential systematic errors associated with fitting models to the BAO signature, which are caused by the modulation of the pattern of linear clustering laid down in the high-redshift Universe by the non-linear scale-dependent growth of structure, the distortions apparent when the signal is observed in redshift space and the bias with which galaxies trace the network of matter fluctuations. However, the fact that the BAOs are imprinted on large, linear and quasi-linear scales of the clustering pattern means that these non-linear, systematic distortions are amenable to analytical or numerical modelling and the leading-order effects are well-understood (Eisenstein, Seo & White 2007; Crocce & Scoccimarro 2008; Matsubara 2008; Sánchez, Baugh & Angulo 2008; Smith, Scoccimarro & Sheth 2008; Seo et al. 2008; Padmanabhan & White 2009). As such, BAOs in current data sets are believed to provide a robust probe of the cosmological model, relatively free of systematic error and dominated by statistical errors. In this sense they provide a powerful cross-check of the distance–redshift relation mapped by SNe.

In this study we report our final analysis of the baryon acoustic peak from the angle-averaged correlation function of the completed WiggleZ Survey data set, in which we present distance-scale measurements as a function of redshift between $z = 0.44$ and $z = 0.73$, including a covariance matrix which may be applied in cosmological parameter fits. We also present a new measurement of the correlation function of the SDSS-LRG sample. We stack the 6dFGS, SDSS-LRG and WiggleZ correlation functions to produce the highest-significance detection to date of the baryon acoustic peak in the galaxy clustering pattern. We perform cosmological parameter fits to this latest BAO distance data set, now comprising data points at six different redshifts. By comparing these fits with those performed on the latest compilation of SNe Ia, we search for systematic disagreements between these two important probes of the distance–redshift relation.

The structure of our paper is as follows. In Section 2 we summarize the three galaxy spectroscopic redshift survey data sets which have provided the most significant BAO measurements. In Section 3 we outline the modelling of the baryon acoustic peak applied in this study. In Section 4 we report the measurement and analysis of the final WiggleZ Survey correlation functions in redshift slices, and in Section 5 we present the new determination of the correlation function of SDSS LRGs. In Section 6 we construct a stacked galaxy correlation function from these surveys and analyse the statistical significance of the BAO detection contained therein. In Section 7 we perform cosmological parameter fits to various combinations of BAO, SNe Ia and CMB data, and we list our conclusions in Section 8.

2 DATA SETS

2.1 The WiggleZ Dark Energy Survey

The WiggleZ Dark Energy Survey (Drinkwater et al. 2010) is a large-scale galaxy redshift survey of bright emission-line galaxies which was carried out at the Anglo-Australian Telescope between 2006 August and 2011 January using the AAOmega spectrograph

(Saunders et al. 2004; Sharp et al. 2006). Targets were selected via joint ultraviolet and optical magnitude and colour cuts using input imaging from the *Galaxy Evolution Explorer* (GALEX) satellite (Martin et al. 2005), the SDSS (York et al. 2000) and the 2nd Red Cluster Sequence (RCS2) Survey (Gilbank et al. 2011). The survey is now complete, comprising approximately 200 000 redshifts and covering of the order of 800 deg^2 of equatorial sky. In this study we analysed a galaxy sample drawn from our final set of observations, after cuts to maximize the contiguity of each survey region. The sample includes a total of $N = 158\,741$ galaxies in the redshift range $0.2 < z < 1.0$.

2.2 The 6-degree Field Galaxy Survey

The 6dFGS (Jones et al. 2009) is a combined redshift and peculiar velocity survey covering nearly the entire southern sky with the exception of a 10° band along the Galactic plane. Observed galaxies were selected from the Two Micron All Sky Survey (2MASS) Extended Source Catalogue (Jarrett et al. 2000) and the redshifts were obtained with the 6-degree Field (6dF) multi-fibre instrument at the UK Schmidt Telescope between 2001 and 2006. The final 6dFGS sample contains 75 117 galaxies distributed over $\sim 17\,000 \text{ deg}^2$ with a mean redshift of $z = 0.052$. The analysis of the baryon acoustic peak in the 6dFGS (Beutler et al. 2011) utilized all galaxies selected to $K \leq 12.9$. We provide a summary of this BAO measurement in Section 6.1.

2.3 The Sloan Digital Sky Survey Luminous Red Galaxy sample

The SDSS included the largest-volume spectroscopic LRG survey to date (Eisenstein et al. 2001). The LRGs were selected from the photometric component of SDSS, which imaged the sky at high Galactic latitude in five passbands u, g, r, i and z (Fukugita et al. 1996; Gunn et al. 1998) using a 2.5-m telescope (Gunn et al. 2006). The images were processed (Lupton et al. 2001; Stoughton et al. 2002; Pier et al. 2003; Ivezić et al. 2004) and calibrated (Hogg et al. 2001; Smith et al. 2002; Tucker et al. 2006), allowing the selection of galaxies, quasars (Richards et al. 2002) and stars for follow-up spectroscopy (Eisenstein et al. 2001; Strauss et al. 2002) with twin fibre-fed double spectrographs. Targets were assigned to plug plates according to a tiling algorithm ensuring nearly complete samples (Blanton et al. 2003).

The LRG sample serves as a good tracer of matter because these galaxies are associated with massive dark matter haloes. The high luminosity of LRGs enables a large volume to be efficiently mapped, and their spectral uniformity makes them relatively easy to identify. In this study we analyse similar LRG catalogues to those presented by Kazin et al. (2010a,b),¹ to which we refer the reader for full details of selection and systematics. In particular, in this study we focus on the sample DR7-Full, which corresponds to all LRGs in the redshift range $0.16 < z < 0.44$ and absolute magnitude range $-23.2 < M_g < -21.2$. The sky coverage and redshift distributions of the LRG samples are presented in Figs 1 and 2 of Kazin et al. (2010a). DR7-Full includes 89 791 LRGs with average redshift ($\langle z \rangle = 0.314$), covering total volume $1.2 h^{-3} \text{ Gpc}^3$ with average number density $8 \times 10^{-5} h^3 \text{ Mpc}^{-3}$.

¹ These catalogues and the associated survey mask are publicly available at <http://cosmo.nyu.edu/~eak306/SDSS-LRG.html>

3 MODELLING THE BARYON ACOUSTIC PEAK

In this section, we summarize the two models we fitted to the new baryon acoustic peak measurements presented in this study. These models describe the quasi-linear effects which cause the acoustic feature and correlation function shape to deviate from the linear-theory prediction. There are two main aspects to model: a damping of the acoustic peak caused by the displacement of matter due to bulk flows, and a distortion in the overall shape of the clustering pattern due to the scale-dependent growth of structure (Eisenstein et al. 2007; Crocce & Scoccimarro 2008; Matsubara 2008; Sánchez et al. 2008; Smith et al. 2008; Seo et al. 2008; Padmanabhan & White 2009). Our models are characterized by four variable parameters: the physical matter density $\Omega_m h^2$ (where Ω_m is the matter density relative to the critical density and $h = H_0/[100 \text{ km s}^{-1} \text{ Mpc}^{-1}]$ is the Hubble parameter), a scale distortion parameter α , a physical damping scale σ_v and a normalization factor b^2 . The models for the correlation function ξ_{model} in terms of separation s can be written in the form

$$\xi_{\text{model}}(s) = b^2 \xi_{\text{fid}}(\Omega_m h^2, \sigma_v, \alpha s). \quad (1)$$

The physical matter density $\Omega_m h^2$ determines (to the first order) both the overall shape of the matter correlation function and the length-scale of the standard ruler by determining the physics before recombination. The scale distortion parameter α relates the distance–redshift relation at the effective redshift of the sample to the fiducial value used to construct the correlation function measurement, in terms of the D_V parameter (Eisenstein et al. 2005; Padmanabhan & White 2008; Kazin, Sánchez & Blanton 2011):

$$D_V(z_{\text{eff}}) = \alpha D_{V,\text{fid}}(z_{\text{eff}}), \quad (2)$$

where D_V is a composite of the physical angular-diameter distance $D_A(z)$ and Hubble parameter $H(z)$, which respectively govern tangential and radial separations in a cosmological model:

$$D_V(z) = \left[(1+z)^2 D_A(z)^2 \frac{cz}{H(z)} \right]^{1/3}. \quad (3)$$

The damping scale σ_v quantifies the typical displacement of galaxies from their initial locations in the density field due to bulk flows, resulting in a ‘washing-out’ of the baryon oscillations at low redshift. The normalization factor b^2 , marginalized in our analysis, models the effects of linear galaxy bias and large-scale redshift-space distortions.

3.1 Default correlation function model

In our first, default, model we constructed the fiducial correlation function ξ_{fid} in equation (1) in a similar manner to Eisenstein et al. (2005) and Blake et al. (2011). First, we generated a linear power spectrum $P_L(k)$ as a function of wavenumber k for a given $\Omega_m h^2$ using the CAMB software package (Lewis, Challinor & Lasenby 2000). We fixed the values of the other cosmological parameters using a fiducial model consistent with the latest fits to the CMB (Komatsu et al. 2011): Hubble parameter $h = 0.71$, physical baryon density $\Omega_b h^2 = 0.0226$, primordial spectral index $n_s = 0.96$ and normalization $\sigma_8 = 0.8$. We also used the fitting formulae of Eisenstein & Hu (1998) to generate a corresponding ‘no-wiggles’ reference spectrum $P_{\text{ref}}(k)$, possessing a similar shape to $P_L(k)$ but with the baryon oscillation component deleted, which we also use in the clustering model as explained below.

We then incorporated the damping of the baryon acoustic peak caused by the displacement of matter due to bulk flows (Eisenstein

et al. 2007; Crocce & Scoccimarro 2008; Matsubara 2008) by interpolating between the linear and reference power spectra using a Gaussian damping term $g(k) \equiv \exp(-k^2 \sigma_v^2)$:

$$P_{\text{damped}}(k) = g(k) P_L(k) + [1 - g(k)] P_{\text{ref}}(k). \quad (4)$$

The magnitude of the damping coefficient σ_v can be estimated for a given value of $\Omega_m h^2$ using the first-order prediction of perturbation theory (Crocce & Scoccimarro 2008):

$$\sigma_v^2 = \frac{1}{6\pi^2} \int P_L(k) dk. \quad (5)$$

However, this relation provides only an approximation to the true non-linear damping (Taruya, Nishimichi & Saito 2010), and we chose to marginalize over σ_v as a free parameter in our analysis. We note that σ_v is closely related to the parameter k_* defined by Sánchez et al. (2008), in the sense that $\sigma_v^2 = 1/2k_*^2$.

We included the boost in small-scale clustering power due to the non-linear scale-dependent growth of structure using the ‘halofit’ prescription of Smith et al. (2003), as applied to the no-wiggles reference spectrum:

$$P_{\text{NL}}(k) = \left[\frac{P_{\text{ref,halofit}}(k)}{P_{\text{ref}}(k)} \right] \times P_{\text{damped}}(k). \quad (6)$$

Finally, we transformed $P_{\text{NL}}(k)$ into the correlation function appearing in equation (1):

$$\xi_{\text{fid}}(s) = \frac{1}{2\pi^2} \int dk k^2 P_{\text{NL}}(k) \left[\frac{\sin(ks)}{ks} \right]. \quad (7)$$

3.2 Comparison correlation function model

The second model we considered for the fiducial correlation function ξ_{fid} , to be compared with the default model described above, was motivated by perturbation theory (Crocce & Scoccimarro 2008; Sánchez et al. 2008):

$$\xi_{\text{fid}}(s) = \xi_L(s) \otimes \exp(-s^2/2\sigma_v^2) + A_{\text{MC}} \frac{d\xi_L(s)}{ds} \xi_1(s). \quad (8)$$

In this relation $\xi_L(s)$ is the linear model correlation function corresponding to the linear power spectrum $P_L(k)$. The symbol \otimes denotes convolution by the Gaussian damping σ_v , which we evaluated as

$$\begin{aligned} \xi_L(s) \otimes \exp(-s^2/2\sigma_v^2) \\ = \frac{1}{2\pi^2} \int dk k^2 P_L(k) \exp(-k^2 \sigma_v^2) \left[\frac{\sin(ks)}{ks} \right], \end{aligned} \quad (9)$$

and ξ_1 is defined by equation (32) in Crocce & Scoccimarro (2008):

$$\xi_1(s) = \frac{1}{2\pi^2} \int dk k P_L(k) j_1(ks), \quad (10)$$

where $j_1(x)$ is the spherical Bessel function of the order of 1. $A_{\text{MC}} = 1$ (fixed in our analysis) is a ‘mode-coupling’ term that restores the small-scale shape of the correlation function and causes a slight shift in the peak position compared to the linear-theory prediction. The model of equation (8) has been shown to yield unbiased results in baryon acoustic peak fits by Sánchez et al. (2008, 2009).

4 WIGGLEZ BARYON ACOUSTIC PEAK MEASUREMENTS IN REDSHIFT SLICES

In this section we describe our measurement and fitting of the baryon acoustic peak in the WiggleZ Survey galaxy correlation function in three overlapping redshift ranges: $0.2 < z < 0.6$, $0.4 < z < 0.8$ and $0.6 < z < 1.0$. Our methodology closely follows that employed by Blake et al. (2011), to which we refer the reader for full details.

4.1 Correlation function measurements

We measured the angle-averaged two-point correlation function $\xi(s)$ for each WiggleZ survey region using the Landy & Szalay (1993) estimator:

$$\xi(s) = \frac{DD(s) - 2DR(s) + RR(s)}{RR(s)}, \quad (11)$$

where $DD(s)$, $DR(s)$ and $RR(s)$ are the data–data, data–random and random–random weighted pair counts in separation bin s , where each random catalogue contains the same number of galaxies as the real data set. We assumed a fiducial flat Λ CDM cosmological model with matter density $\Omega_m = 0.27$ to convert the galaxy redshifts and angular positions to spatial comoving co-ordinates. In the construction of the pair counts each data or random galaxy i was assigned a weight $w_i = 1/(1 + n_i P_0)$, where n_i is the survey number density at the location of the i th galaxy (determined by averaging over many random catalogues) and $P_0 = 5000 h^{-3} \text{Mpc}^3$ is a characteristic power spectrum amplitude at the physical scales of interest. The DR and RR pair counts were determined by averaging over 10 random catalogues, which were constructed using the selection-function methodology described by Blake et al. (2010). We measured the correlation function in $10 h^{-1} \text{Mpc}$ separation bins in three overlapping redshift slices $0.2 < z < 0.6$, $0.4 < z < 0.8$ and $0.6 < z < 1.0$. The effective redshift z_{eff} of the correlation function measurement in each slice was determined as the weighted mean redshift of the galaxy pairs in the separation bin $100 < s < 110 h^{-1} \text{Mpc}$, where the redshift of a pair is simply the average $(z_1 + z_2)/2$, and the weighting is $w_1 w_2$ where w_i is as defined above. For the three redshift slices in question we obtained values $z_{\text{eff}} = 0.44$, 0.60 and 0.73 .

We determined the covariance matrix of the correlation function measurement in each survey region using an ensemble of 400 lognormal realizations, using the method described by Blake et al. (2011). Lognormal realizations provide a reasonably accurate galaxy clustering model for the linear and quasi-linear scales which are important for the modelling of baryon oscillations. They are more reliable than jack-knife errors, which provide a poor approximation for the correlation function variance on BAO scales because the pair separations of interest are usually comparable to the size of the jack-knife regions, which are then not strictly independent. We note that the lognormal covariance matrix only includes the effects of the survey window function, and neglects the covariance due to the non-linear growth of structure and redshift-space effects. The full non-linear covariance matrix may be studied with the aid of a large set of N -body simulations (Rimes & Hamilton 2005; Takahashi et al. 2011). Work is in progress to construct such a simulation set for WiggleZ galaxies, although this is a challenging computational problem because the typical dark matter haloes hosting the star-forming galaxies mapped by WiggleZ are ~ 20 times lower in mass than the LRG sample described in Section 5, requiring high-resolution large-volume simulations. However, we note that Takahashi et al. (2011) demonstrated that the impact of using the full non-linear covariance matrix on the accuracy of extraction of BAOs is small, so we do not expect our measurements to be compromised significantly through using lognormal realizations to estimate the covariance matrix.

We combined the correlation function measurements and corresponding covariance matrices for the different survey regions using optimal inverse-variance weighting in each separation bin (see equations 8 and 9 in White et al. 2011):

$$\xi_{\text{comb}} = \mathbf{C}_{\text{comb}} \sum_{\text{regions } n} \mathbf{C}_n^{-1} \xi_n, \quad (12)$$

$$\mathbf{C}_{\text{comb}}^{-1} = \sum_{\text{regions } n} \mathbf{C}_n^{-1}. \quad (13)$$

In these equations, ξ_n and ξ_{comb} are vectors representing the correlation function measurements in region n and the optimally combined correlation function, and \mathbf{C}_n and \mathbf{C}_{comb} are the covariance matrices corresponding to these two measurement vectors (with inverses \mathbf{C}_n^{-1} and $\mathbf{C}_{\text{comb}}^{-1}$). This method produces an almost identical result to combining the individual pair counts and then estimating the correlation function using equation (11). The combined correlation functions in the three redshift slices are displayed in Fig. 1, together with a total WiggleZ correlation function for the whole redshift range $0.2 < z < 1.0$ which was constructed by combining the separate measurements for $0.2 < z < 0.6$ and $0.6 < z < 1.0$. The corresponding lognormal covariance matrices for each measurement are shown in Fig. 2.

4.2 Parameter fits

We fitted the first, default correlation function model described in Section 3 to the WiggleZ measurements in redshift slices $0.2 < z < 0.6$, $0.4 < z < 0.8$ and $0.6 < z < 1.0$, varying $\Omega_m h^2$, α , σ_v and b^2 . Our default fitting range was $10 < s < 180 h^{-1} \text{Mpc}$ (following Eisenstein et al. 2005), where $10 h^{-1} \text{Mpc}$ is an estimate of the minimum scale of validity for the quasi-linear theory described in Section 3. This minimum scale is a quantity which depends on the survey redshift and galaxy bias (which control the amplitude of the non-linear, scale-dependent contributions to the shape of the correlation function) together with the signal-to-noise ratio of the measurement. When fitting equation (7) to the WiggleZ Survey correlation function we find no evidence for a systematic variation in the derived BAO parameters when we vary the minimum fitted scale over the range $10 \leq s_{\text{min}} \leq 50 h^{-1} \text{Mpc}$.

We minimized the χ^2 statistic using the full data covariance matrix derived from lognormal realizations. The fitting results, including the marginalized parameter measurements, are displayed in Table 1. The minimum values of χ^2 for the model fits in the three redshift slices were 11.4, 10.1 and 13.7 for 13 degrees of freedom (d.o.f.), indicating that our model provides a good fit to the data. The best-fitting scale distortion parameters, which provide the value of $D_V(z_{\text{eff}})$ for each redshift slice, are all consistent with the fiducial distance–redshift model (a flat Λ CDM universe with $\Omega_m = 0.27$) with marginalized errors of 9.1 per cent, 6.5 per cent and 6.4 per cent in the three redshift slices. The best-fitting matter densities $\Omega_m h^2$ are consistent with the latest analyses of the CMB (Komatsu et al. 2011). The damping parameters σ_v are not well-constrained using our data, but the allowed range is consistent with the predictions of equation (5) for our fiducial model [which are $\sigma_v = (4.8, 4.5, 4.2) h^{-1} \text{Mpc}$ for the three redshift slices]. When fitting σ_v we only permit it to vary over the range $\sigma_v \geq 0$.

The 2D probability contours for $\Omega_m h^2$ and α , marginalizing over σ_v and b^2 , are displayed in Fig. 3. The measurement of α (hence $D_V = \alpha D_{V,\text{fid}}$) is significantly correlated with the matter density, which controls the shape of the clustering pattern.

We indicate three degeneracy directions in the parameter space of Fig. 3. The first direction (the dashed line) corresponds to a constant measured acoustic peak separation, i.e. $\alpha/r_s(z_d) = \text{constant}$, where $r_s(z_d)$ is the sound horizon at the drag epoch as a function of $\Omega_m h^2$, determined using the fitting formula quoted in equation (12) of Percival et al. (2010). This parameter degeneracy would be expected in the case that just the baryon acoustic peak is driving the model fits,

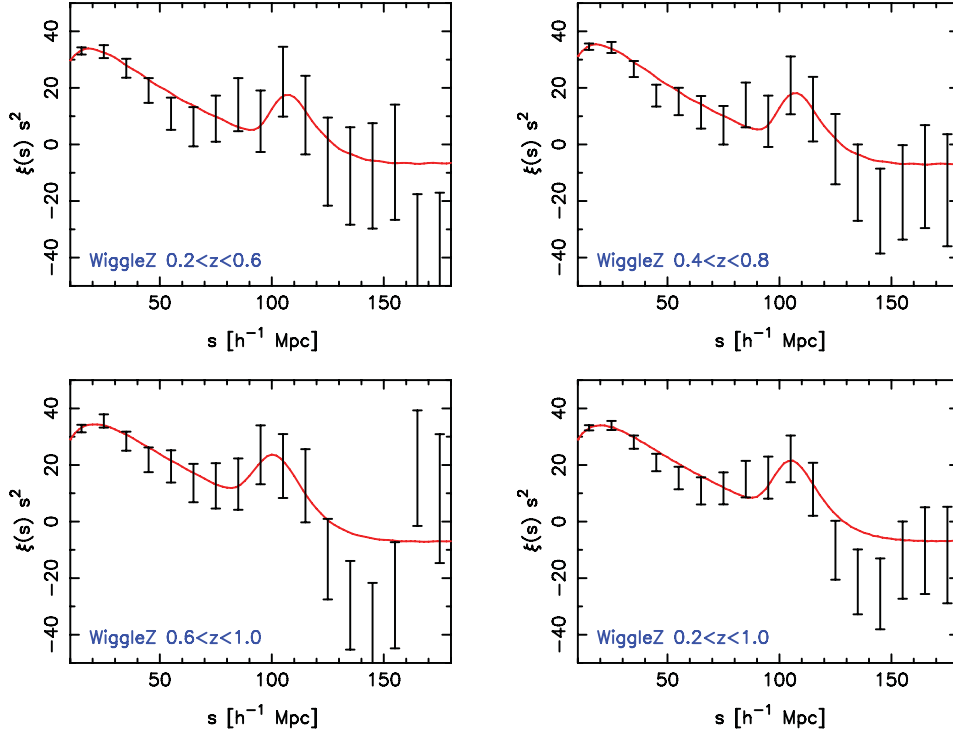


Figure 1. Measurements of the galaxy correlation function $\xi(s)$, combining different WiggleZ survey regions, for the redshift ranges $0.2 < z < 0.6$, $0.4 < z < 0.8$, $0.6 < z < 1.0$ and $0.2 < z < 1.0$, plotted in the combination $s^2 \xi(s)$ where s is the comoving redshift-space separation. The best-fitting clustering models in each case, varying the parameters $\Omega_m h^2$, α , σ_v and b^2 as described in Section 3, are overlotted as the solid lines. Significant detections of the baryon acoustic peak are obtained in each separate redshift slice.

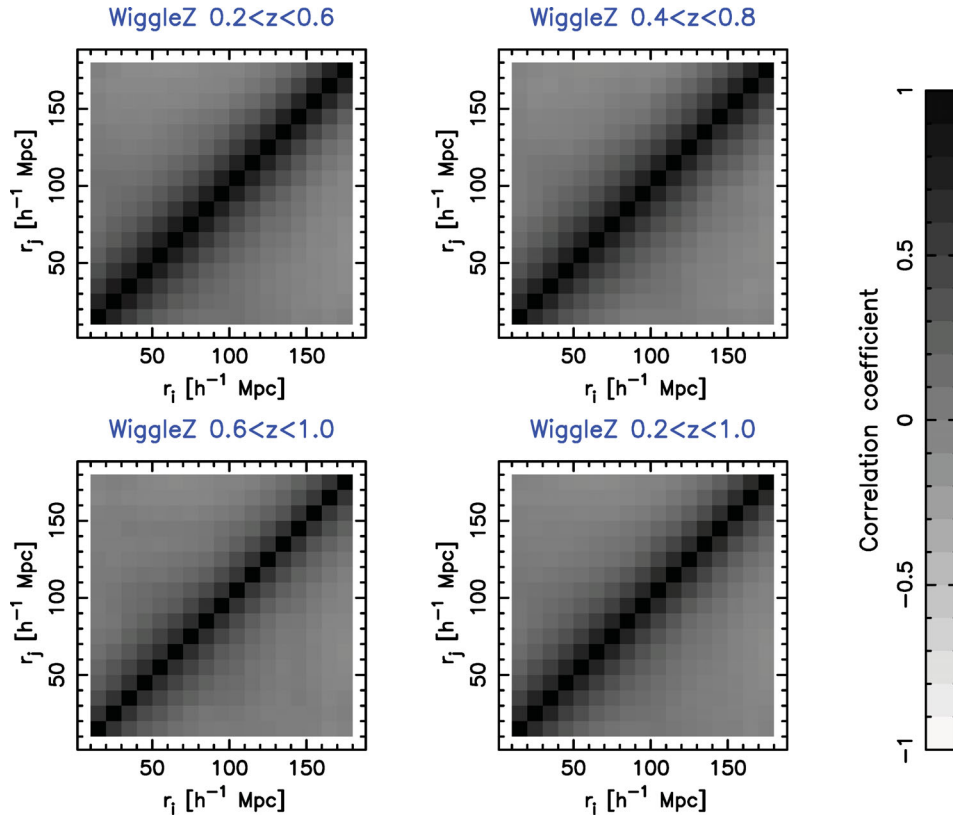


Figure 2. The amplitude of the cross-correlation $C_{ij} / \sqrt{C_{ii} C_{jj}}$ of the covariance matrix C_{ij} for the combined WiggleZ correlation function measurements for the redshift ranges $0.2 < z < 0.6$, $0.4 < z < 0.8$, $0.6 < z < 1.0$ and $0.2 < z < 1.0$, determined using lognormal realizations.

Table 1. Results of fitting the four-parameter model ($\Omega_m h^2, \alpha, \sigma_v, b^2$) to the WiggleZ correlation functions in three redshift slices, together with the results for the full sample. The effective redshifts of the measurement in each slice are listed in Column 2, and the corresponding values of D_V for the fiducial cosmological model appear in Column 3. The values of χ^2 for the best-fitting models are quoted in Column 4, for 13 d.o.f. Columns 5, 6 and 7 show the marginalized measurements of the matter density parameter $\Omega_m h^2$, scale distortion parameter α and damping scale σ_v in each redshift slice. Corresponding measurements of the BAO distilled parameters $A(z)$ and d_z are displayed in Columns 8 and 9. The measured values of D_V in each redshift slice are given by $\alpha D_{V,\text{fid}}$.

Sample	z_{eff}	$D_{V,\text{fid}}$ (Mpc)	χ^2	$\Omega_m h^2$	α	σ_v (h^{-1} Mpc)	$A(z_{\text{eff}})$	$d_{z,\text{eff}}$
WiggleZ – $0.2 < z < 0.6$	0.44	1617.8	11.4	0.143 ± 0.020	1.024 ± 0.093	4.5 ± 3.5	0.474 ± 0.034	0.0916 ± 0.0071
WiggleZ – $0.4 < z < 0.8$	0.60	2085.4	10.1	0.147 ± 0.016	1.003 ± 0.065	4.1 ± 3.4	0.442 ± 0.020	0.0726 ± 0.0034
WiggleZ – $0.6 < z < 1.0$	0.73	2421.9	13.7	0.120 ± 0.013	1.113 ± 0.071	4.4 ± 3.2	0.424 ± 0.021	0.0592 ± 0.0032
WiggleZ – $0.2 < z < 1.0$	0.60	2085.4	11.5	0.127 ± 0.011	1.071 ± 0.053	4.4 ± 3.3	0.441 ± 0.017	0.0702 ± 0.0032

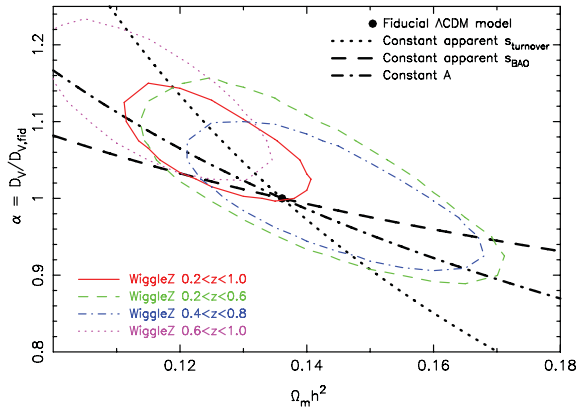


Figure 3. Probability contours of the physical matter density $\Omega_m h^2$ and scale distortion parameter α obtained by fitting to the WiggleZ survey combined correlation function in four redshift ranges $0.2 < z < 0.6$, $0.4 < z < 0.8$, $0.6 < z < 1.0$ and $0.2 < z < 1.0$. The heavy dashed and dotted lines are the degeneracy directions which are expected to result from fits involving respectively just the acoustic peak, and just the shape of a pure CDM power spectrum. The heavy dash-dotted line represents a constant value of the acoustic ‘A’ parameter defined by equation (14), which is the parameter best measured by the WiggleZ correlation function data. The solid circle represents the location of our fiducial cosmological model. The contour level in each case encloses regions containing 68.27 per cent of the total likelihood.

such that the measured low-redshift distance $\alpha D_{V,\text{fid}}$ is proportional to the standard ruler scale $r_s(z_d)$.

The second direction (the dotted line) illustrated in Fig. 3 represents the degeneracy resulting from a constant measured shape of a cold dark matter (CDM) power spectrum, i.e. $\Omega_m h^2 \times \alpha = \text{constant}$. We note here the consistency between this scaling and the ‘shape parameter’ $\Gamma = \Omega_m h$ used to parametrize the CDM transfer function (Bardeen et al. 1986). This shape parameter assumes that wavenumbers are observed in units of $h \text{Mpc}^{-1}$, but the standard ruler scale encoded in BAOs is calibrated by the CMB in units of Mpc, with no factor of h .

The third direction (the dash-dotted line) shown in Fig. 3, which best describes the degeneracy in our data, corresponds to a constant value of the acoustic parameter $A(z)$ introduced by Eisenstein et al. (2005),

$$A(z) \equiv \frac{100 D_V(z) \sqrt{\Omega_m h^2}}{c z}, \quad (14)$$

which appears in Fig. 3 as $\sqrt{\Omega_m h^2} \times \alpha = \text{constant}$. We note that the values of $A(z)$ predicted by any cosmological model are independent of h , because D_V is proportional to h^{-1} .

The acoustic parameter $A(z)$ provides the most appropriate description of the distance–redshift relation determined by a BAO measurement in which both the clustering shape and acoustic peak are contributing towards the fit, such that the whole correlation function is being used as a standard ruler (Eisenstein et al. 2005; Sánchez et al. 2008; Shoji, Jeong & Komatsu 2009). In this case, the resulting measurement of $A(z)$ is approximately uncorrelated with $\Omega_m h^2$. We repeated our BAO fit to the WiggleZ correlation functions in redshift slices using the parameter set $(A, \Omega_m h^2, \sigma_v, b^2)$. The marginalized values of $A(z)$ we obtained are quoted in Table 1, and correspond to measurements of the acoustic parameter with accuracies 7.2 per cent, 4.5 per cent and 5.0 per cent in the three redshift slices.

We also fitted our data with the parameter set $(d_z, \Omega_m h^2, \sigma_v, b^2)$, where $d_z \equiv r_s(z_d)/D_V(z)$. Results are again listed in Table 1, corresponding to measurements of d_z with accuracies 7.8 per cent, 4.7 per cent and 5.4 per cent in the three redshift slices. We note that, unlike for the case of $A(z)$, these measurements of d_z are correlated with the matter density $\Omega_m h^2$, due to the orientation of the parameter degeneracy directions in Fig. 3 (noting that constant d_z corresponds to the ‘constant measured acoustic peak’ case defined above).

As a check for systematic modelling errors, we repeated the fits to the WiggleZ correlation functions using the second acoustic peak model described in Section 3, motivated by perturbation theory, fitting the data over the same range of scales. The marginalized measurements of α in the three redshift slices were $(1.032 \pm 0.093, 0.981 \pm 0.060, 1.091 \pm 0.079)$, to be compared with the results for the default model quoted in Table 1. The amplitude of the systematic error in the fitted scale distortion parameter is hence significantly lower than the statistical error in the measurement (by at least a factor of 3 in all cases).

We assessed the statistical significance of the BAO detections in each redshift slice by repeating the parameter fits replacing the model correlation function with one generated using the ‘no-wiggles’ reference power spectrum $P_{\text{ref}}(k)$ as a function of $\Omega_m h^2$ (Eisenstein & Hu 1998). The minimum values obtained for the χ^2 statistic for the fits in the three redshift slices were 15.2, 15.1 and 19.4, indicating that the model containing baryon oscillations was favoured by $\Delta\chi^2 = 3.8, 5.0$ and 5.7 (with the same number of parameters fitted). These intervals correspond to detections of the baryon acoustic peaks in the redshift slices with statistical significances between 1.9σ and 2.4σ . We note that the marginalized uncertainty in the scale distortion parameter for the no-wiggles model fit degrades by a factor of between 2 and 3 compared to

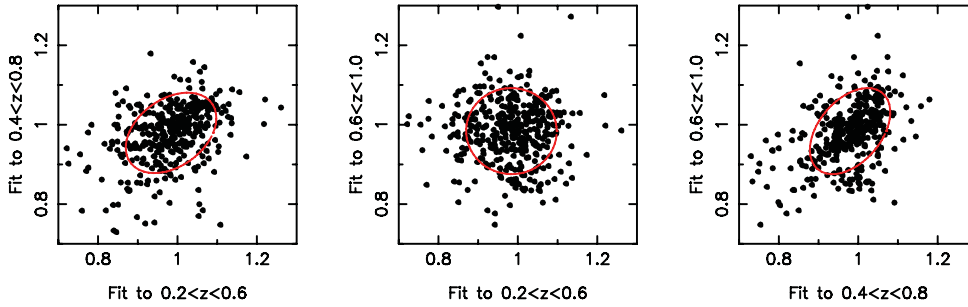


Figure 4. These panels illustrate the correlations between the scale distortion parameters α fitted to correlation functions for three overlapping WiggleZ redshift slices using 400 lognormal realizations. The red ellipses represent the derived correlation coefficients between these measurements.

the fit to the full model, demonstrating that the acoustic peak is very important for establishing the distance constraints from our measurements.

We used the same approach to determine the statistical significance of the BAO detection in the full WiggleZ redshift span $0.2 < z < 1.0$, after combining the correlation function measurements in the redshift slices $0.2 < z < 0.6$ and $0.6 < z < 1.0$. In this case the model containing baryon oscillations was favoured by $\Delta\chi^2 = 7.7$, corresponding to a statistical significance of 2.8σ for the detection of the baryon acoustic peak.

4.3 Covariances between redshift slices

We used the ensemble of lognormal realizations to quantify the covariance between the BAO measurements in the three overlapping WiggleZ redshift slices. For each of the 400 lognormal realizations in every WiggleZ region, we measured correlation functions for the redshift ranges $\Delta z_1 \equiv 0.2 < z < 0.6$, $\Delta z_2 \equiv 0.4 < z < 0.8$ and $\Delta z_3 \equiv 0.6 < z < 1.0$ and combined these correlation functions for the different regions using inverse-variance weighting. We then fitted the default clustering model described in Section 3 to each of the 400 combined correlation functions for the three redshift slices.

Fig. 4 displays the correlations between the 400 marginalized values of the scale distortion parameter α for every pair of redshift slices. As expected, significant correlations are found in the values of α obtained from fits to the overlapping redshift ranges ($\Delta z_1, \Delta z_2$) and ($\Delta z_2, \Delta z_3$), whereas the fits to the non-overlapping pair ($\Delta z_1, \Delta z_3$) produce an uncorrelated measurement (within the statistical noise). The corresponding correlation coefficients for the overlapping pairs are $\rho_{12} = 0.369$ and $\rho_{23} = 0.438$, where $\rho_{ij} \equiv C_{ij} / \sqrt{C_{ii}C_{jj}}$ in terms of the covariances $C_{ij} \equiv \langle \alpha_i \alpha_j \rangle - \langle \alpha_i \rangle \langle \alpha_j \rangle$. Table 2 contains the resulting inverse covariance matrix for the measurements of $A(z)$ in the three redshift slices, which should be used in cosmological parameter fits.

4.4 Comparison to mock galaxy catalogue

As a further test for systematic errors in our distance scale measurements we fitted our BAO models to a dark matter halo catalogue generated as part of the Gigaparsec WiggleZ (GiggleZ) simulation suite (Poole et al., in preparation). The main GiggleZ simulation consists of a 2160³ particle dark matter N -body calculation spanning a cosmological box of side $1 h^{-1}$ Gpc. The cosmological parameters used for the simulation initial conditions were $[\Omega_m, \Omega_b, n_s, h, \sigma_8] = [0.273, 0.0456, 0.96, 0.705, 0.812]$.

We measured the redshift–space correlation function of a mass-limited subset of the dark matter halo catalogue extracted from

Table 2. The inverse covariance matrix \mathbf{C}^{-1} of the measurements from the WiggleZ survey data of the acoustic parameter $A(z)$ defined by equation (14). We have performed these measurements in three overlapping redshift slices $0.2 < z < 0.6$, $0.4 < z < 0.8$ and $0.6 < z < 1.0$ with effective redshifts $z_{\text{eff}} = 0.44, 0.6$ and 0.73 , respectively. The data vector is $\mathbf{A}_{\text{obs}} = (0.474, 0.442, 0.424)$, as listed in Table 1. The chi-squared statistic for any cosmological model vector \mathbf{A}_{mod} can be obtained via the matrix multiplication $\chi^2 = (\mathbf{A}_{\text{obs}} - \mathbf{A}_{\text{mod}})^T \mathbf{C}^{-1} (\mathbf{A}_{\text{obs}} - \mathbf{A}_{\text{mod}})$. The matrix is symmetric; we just quote the upper diagonal.

Redshift slice	$0.2 < z < 0.6$	$0.4 < z < 0.8$	$0.6 < z < 1.0$
$0.2 < z < 0.6$	1040.3	−807.5	336.8
$0.4 < z < 0.8$		3720.3	−1551.9
$0.6 < z < 1.0$			2914.9

the $z = 0.6$ snapshot. This subset of dark matter haloes, spanning a small range of maximum circular velocities around 125 km s^{-1} , was selected such that its large-scale clustering amplitude was similar to the WiggleZ galaxies at that redshift. We obtained the covariance matrix of the measurement using jack-knife techniques. We fitted our default correlation function model described in Section 3 to the result, varying $\Omega_m h^2$, α , σ_v and b^2 and using the same fitting range as the WiggleZ measurement, $10 < s < 180 h^{-1}$ Mpc.

Fig. 5 shows the $z = 0.6$ GiggleZ halo correlation function measurement compared to the WiggleZ correlation function for the redshift range $0.4 < z < 0.8$ (which was plotted in the top-right panel of Fig. 1). We overplot the best-fitting default correlation function model for the GiggleZ data. The 2D probability contours for $\Omega_m h^2$ and α are displayed in Fig. 6, again compared to the $0.4 < z < 0.8$ WiggleZ measurement and indicating the same degeneracy directions as shown in Fig. 3. We conclude that the best-fitting parameter values are consistent with the input values of the simulation (within the statistical error expected in a measurement that uses a single realization) and there is no evidence for significant systematic error. We note that the effective volume of the halo catalogue is slightly greater than that of the WiggleZ survey redshift range $0.4 < z < 0.8$; hence the BAO measurements are more accurate in the case of GiggleZ.

5 BARYON ACOUSTIC PEAK MEASUREMENT FROM THE FULL SLOAN DIGITAL SKY SURVEY LUMINOUS RED GALAXY SAMPLE

In this section, we measure and fit the correlation function of the SDSS-LRG DR7-Full sample. This analysis is similar to that performed by Kazin et al. (2010a) for quasi-volume-limited subsamples

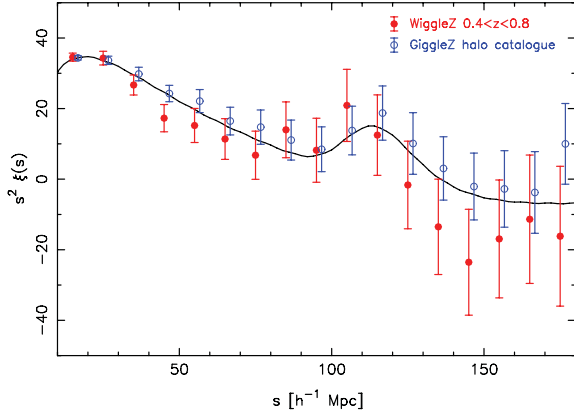


Figure 5. Measurement of the galaxy correlation function $\xi(s)$ from a GigggleZ redshift-space halo subset at $z = 0.6$, chosen to possess a similar large-scale clustering amplitude to the WiggleZ galaxies at that redshift. We plot the correlation function in the combination $s^2 \xi(s)$ where s is the comoving redshift-space separation, and compare the result to the WiggleZ correlation function for the redshift range $0.4 < z < 0.8$. The best-fitting clustering model to the GigggleZ measurement, varying the parameters $\Omega_m h^2$, α , σ_v and b^2 as described in Section 3, is overplotted as the solid line.

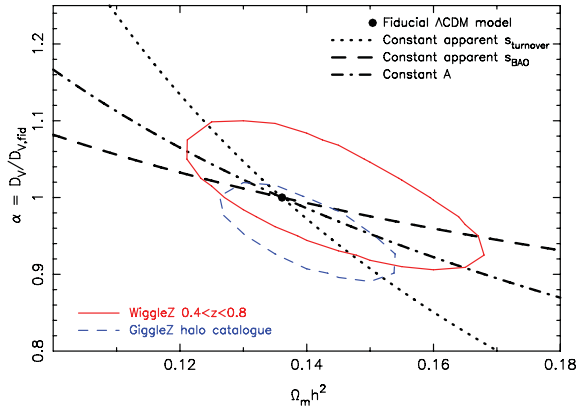


Figure 6. Probability contours of the physical matter density $\Omega_m h^2$ and scale distortion parameter α obtained by fitting the default correlation function model to the GigggleZ halo subset at $z = 0.6$. We compare the result to the WiggleZ measurement in the redshift range $0.4 < z < 0.8$ and overplot the same degeneracy directions as shown in Fig. 3. The solid circle represents the location of our fiducial cosmological model. The contour level in each case encloses regions containing 68.27 per cent of the total likelihood.

with $z < 0.36$, but now extended to a higher maximum redshift $z = 0.44$. We note that we assume a fiducial cosmology $\Omega_m = 0.25$ for this analysis, motivated by the cosmological parameters used in the Large Suite of Dark Matter Simulations (LasDamas) simulations (which we use to determine the covariance matrix of the measurement as described in Section 5.2). The choice instead of $\Omega_m = 0.27$, as used for the 6dFGS and WiggleZ analyses, would yield very similar results because the Alcock–Paczynski distortion between these cases is negligible compared to the statistical errors in α .

5.1 Correlation function measurement

We measured the correlation function of the SDSS-LRG DR7-Full sample by applying the estimator of equation (11), using random catalogues constructed in the manner described in detail by Kazin et al. (2010a). For the purposes of the model fits in this section we

used separation bins of width $6.6 h^{-1}$ Mpc spanning the range $40 < s < 200 h^{-1}$ Mpc, although we also determined results in $10 h^{-1}$ Mpc bins in order to combine with the 6dFGS and WiggleZ correlation functions in Section 6. The measurement of the DR7-Full correlation function in $6.6 h^{-1}$ Mpc bins is displayed in the left-hand panel of Fig. 7, where the error bars are determined from the diagonal elements of the covariance matrix of 160 mock realizations, generated as described in Section 5.2. The solid and dashed lines in Fig. 7 are two best-fitting models, determined as explained in Section 5.3.

The correlation function measurements in the separation range $120 < s < 190 h^{-1}$ Mpc are higher than expected in the best-fitting model. However, it is important to remember that these data points are correlated. The reduced chi-squared statistics corresponding to these models are $\chi^2/\text{d.o.f.} = 1.1\text{--}1.2$ (for 22 d.o.f.), which fall well within the distribution of χ^2 found in individual fits to the 160 mock catalogues, as shown in the right-hand inset in Fig. 7. Kazin et al. (2010a) discussed the excess clustering measurement in SDSS-LRG subsamples and suggested that this is likely to result from sample variance. This is now reinforced by the fact that the independent-volume measurements from the WiggleZ and 6dFGS samples do not show similar trends of excess (see Fig. 8).

A potential cause of the stronger-than-expected clustering of LRGs on large scales is the effect of not masking faint stars on random catalogue generation. Ross et al. (2011) showed that apparent excess large-scale angular clustering measured in photometric LRG samples (Blake et al. 2007; Padmanabhan et al. 2007; Thomas, Abdalla & Lahav 2011) is a systematic effect imprinted by anti-correlations between faint stars and the galaxies, which can be corrected for by masking out regions around the stars. However, in the sparser SDSS-DR7 LRG sample the faint stars are uncorrelated with the galaxies at the angles of interest and do not introduce significant systematic errors in the measured correlation function (A. Sánchez, private communication).

5.2 LasDamas mock galaxy catalogues

We simulated the SDSS-LRG correlation function measurement and determined its covariance matrix using the mock galaxy catalogues provided by the LasDamas (McBride et al., in preparation). These N -body simulations were generated using cosmological parameters consistent with the *Wilkinson Microwave Anisotropy Probe* (WMAP) 5-year fits to the CMB fluctuations (Komatsu et al. 2009): $[\Omega_m, \Omega_b, n_s, h, \sigma_8] = [0.25, 0.04, 1.0, 0.7, 0.8]$.

The LasDamas collaboration generated realistic LRG mock catalogues² by placing galaxies inside dark matter haloes using a Halo Occupation Distribution (HOD; Berlind & Weinberg 2002). The HOD parameters were chosen to reproduce the observed galaxy number density as well as the projected two-point correlation function $w_p(r_p)$ of the SDSS-LRG sample at separations $0.3 < r_p < 30 h^{-1}$ Mpc. We used a suite of 160 LRG mock catalogues constructed from light cone samples with a mean number density $\bar{n} \sim 10^{-4} h^3 \text{Mpc}^{-3}$. Each DR7-Full mock catalogue covers the redshift range $0.16 < z < 0.44$ and reproduces the SDSS angular mask, corresponding to a total volume $1.2 h^{-3} \text{Gpc}^3$. The mock catalogues were subsampled to match the observed redshift distribution of the LRGs.

² <http://lss.phy.vanderbilt.edu/lasdamas/>

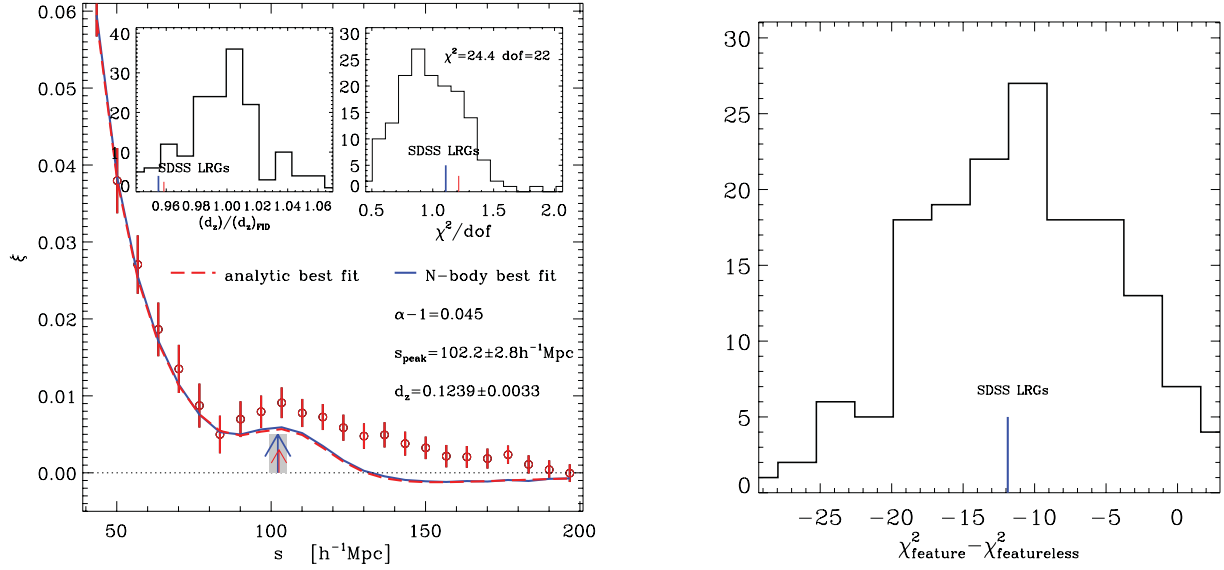


Figure 7. The left-hand plot displays our correlation function measurement for the SDSS-LRG DR7-Full sample over the separation range $40 < s < 200 h^{-1} \text{ Mpc}$ (where the error bars are the diagonal elements of the covariance matrix determined from 160 mock realizations). The solid line is the best-fitting model based on the mock-mean correlation function ξ_{mean} , and the dashed line is the best-fitting analytic perturbation-theory model correlation function ξ_{pt} based on equation (8). The arrows point to the most likely peak position according to each model, where the longer arrow corresponds to the ξ_{mean} result $s_{\text{peak}} = 102.2 \pm 2.8 h^{-1} \text{ Mpc}$. In the right-hand inset the reduced chi-squared statistic $\chi^2/\text{d.o.f.} = 1.1$ (1.2) using ξ_{mean} (ξ_{pt}) for 22 d.o.f. is compared with a histogram of the results fitting to the 160 individual mock realizations. The left-hand inset compares the measurement of $d_z = 0.314$ to the distribution found from the mocks; the offset of the measured result is due to the fact that the fiducial matter density $\Omega_m = 0.25$ used to generate the mocks is a little lower than the current best fits to cosmological data. The right-hand plot shows the distribution amongst the 160 mocks of the difference in the chi-squared statistic between a model containing the baryon acoustic peak and a featureless model. The 3.4σ detection of the baryon acoustic feature that we find in DR7-Full ($\Delta\chi^2 = 11.9$) falls well within the distribution of values found by applying a similar analysis to the mock catalogues.

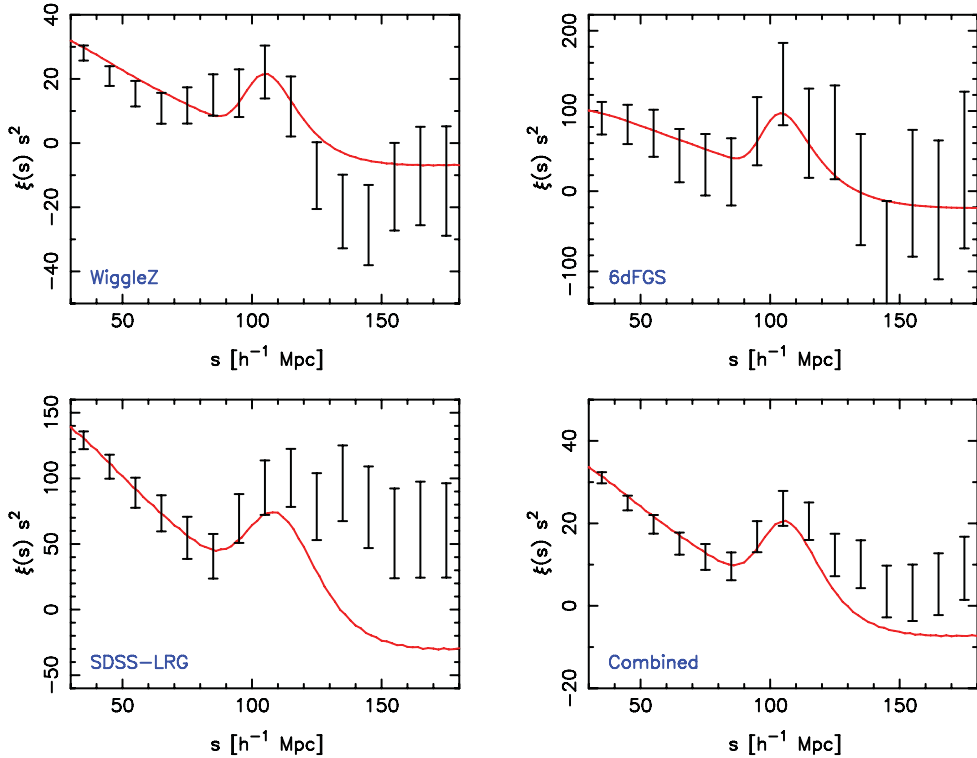


Figure 8. The correlation function measurements $\xi(s)$ for the WiggleZ, SDSS-LRG and 6dFGS galaxy samples, plotted in the combination $s^2 \xi(s)$ where s is the comoving redshift–space separation. The lower-right panel shows the combination of these measurements with inverse-variance weighting. The best-fitting clustering models in each case, varying the parameters $\Omega_m h^2$, α , σ_v and b^2 as described in Section 3, are overlotted as the solid lines.

5.3 Correlation function modelling

We extracted the scale of the baryon acoustic feature in the DR7-Full correlation function measurement by fitting for the scale distortion parameter α relative to a template correlation function ξ_{fid} using equation (1), fitting over the separation range $40 < s < 200 h^{-1}$ Mpc. Together with the two correlation function models already described in Section 3, the availability of the suite of LasDamas mock catalogues allows us to add a third template to use as ξ_{fid} : the mock-mean correlation function ξ_{mean} of all 160 realizations, which includes effects due to the non-linear growth of structure, redshift-space distortions, galaxy bias, light-coning and the observed 3D mask.

The best-fitting model taking $\xi_{\text{fid}} = \xi_{\text{mean}}$, marginalizing over the correlation function amplitude, is displayed as the solid line in Fig. 7, corresponding to $\alpha = 1.045$. The χ^2 statistic of the best fit is 24.2 (for 22 d.o.f.). The most likely baryon acoustic peak position (determined using the method of Kazin et al. 2010a) is $s_{\text{peak}} = 102.2 \pm 2.8 h^{-1}$ Mpc (represented by the large arrow in Fig. 7), where the quoted error is based on the sample variance determined by performing the same analysis on all 160 mock catalogues. The corresponding measurement of the distilled BAO parameter is $d_{z=0.314} = 0.1239 \pm 0.0033$. The distribution of measurements of d_z for the 160 mocks is shown as the left-hand inset in Fig. 7. We do not expect the SDSS result (vertical lines) to coincide with unity, because of the difference between the true and fiducial cosmological parameters.

As a comparison, we also fitted to these data the two correlation function models described in Section 3, parametrized by $(d_z, \Omega_m h^2, \sigma_v, b^2)$. The marginalized measurements of d_z for the two models were 0.1265 ± 0.0048 and 0.1272 ± 0.0050 , consistent with our determination based on the mock-mean correlation function (which effectively uses fixed values of $\Omega_m h^2$ and σ_v).

Our best-fitting analytic perturbation-theory model due to Crocce & Scoccimarro (2008) is displayed as the red dashed line in the left-hand panel of Fig. 7. In this model we find that the best-fitting value of s_{peak} is correlated with σ_v , although such changes produce offsets smaller than the 1σ statistical error in α (represented by the grey region around the short arrows in Fig. 7).

5.4 Significance of detection of the SDSS-LRG baryon acoustic feature

We assessed the statistical significance of the detection of the baryon acoustic peak in the SDSS-LRG sample in a similar style to the WiggleZ analysis described in Section 4.2, by comparing the best-fitting values of χ^2 for models containing a baryon acoustic feature (χ^2_{feature}) and featureless models ($\chi^2_{\text{featureless}}$) constructed using the ‘no-wiggles’ power spectrum of Eisenstein & Hu (1998). We used the perturbation-theory model for the baryon acoustic peak described in Section 3 when constructing these models.

The SDSS-LRG data set produced $\Delta\chi^2 = \chi^2_{\text{feature}} - \chi^2_{\text{featureless}} = -11.9$ over the separation range $40 < s < 200 h^{-1}$ Mpc, corresponding to a detection of the baryon acoustic feature with significance of 3.4σ . The histogram resulting from repeating this analysis for all 160 mocks is displayed in the right-hand panel of Fig. 7, following Cabre & Gaztanaga (2011); we see that the SDSS result is as expected from an average realization.

We used the same method to compare the significance of detection of the acoustic peak in DR7-Full with that obtained in the volume-limited LRG subsamples analysed by Kazin et al. (2010a). The sample ‘DR7-Sub’, a quasi-volume-limited LRG catalogue spanning redshift range $0.16 < z < 0.36$ and luminosity range $-23.2 <$

$M_g < -21.2$, yields a detection significance of 2.2σ . For the sample ‘DR7-Bright’, a sparser volume-limited catalogue with a brighter luminosity cut $-23.2 < M_g < -21.8$, the significance of the baryon acoustic feature is just below 2σ .

6 THE STACKED BARYON ACOUSTIC PEAK

Our goal in this section is to assess the overall statistical significance with which the baryon acoustic peak is detected in the combination of current galaxy surveys. In order to do this, we combined the galaxy correlation functions measured from the WiggleZ Survey, the SDSS-LRG sample and the 6dFGS, and fitted the models described in Section 3 to the result. Although we acknowledge that model fits to a combination of correlation functions obtained using different redshifts and galaxy types will produce parameter values that evade an easy physical interpretation, the resulting statistical significance of the BAO detection remains a quantity of interest.

6.1 The 6dFGS baryon acoustic peak measurement

For completeness, we summarize here the measurement of the baryon acoustic peak from the 6dFGS reported by Beutler et al. (2011). After optimal weighting of the data to minimize the correlation function error at the baryon acoustic peak, the 6dFGS sample covered an effective volume $V_{\text{eff}} = 0.08 h^{-3} \text{ Gpc}^3$ with effective redshift $z_{\text{eff}} = 0.106$. Beutler et al. fitted the model defined by our equation (8) to the 6dFGS correlation function, using lognormal realizations to determine the data covariance matrix and varying the parameter set $\Omega_m h^2, \alpha, \sigma_v$ and b^2 . The model fits were performed over the separation range $10 < s < 190 h^{-1}$ Mpc, with checks made that the best-fitting parameters were not sensitive to the minimum separation employed. The resulting measurements of the distance scale were quantified as $D_V(0.106) = 457 \pm 27$ Mpc, $d_{0.106} = 0.336 \pm 0.015$ or $A(0.106) = 0.526 \pm 0.028$. The statistical significance of the detection of the acoustic peak was estimated to be 2.4σ , based on the difference in chi-squared $\Delta\chi^2 = 5.6$ between the best-fitting model and the corresponding best fit of a zero-baryon model.

6.2 The combined correlation function

Fig. 8 displays the three survey correlation functions combined in our study: the WiggleZ $0.2 < z < 1.0$ measurement plotted in the lower-right panel of Fig. 1, the 6dFGS correlation function reported by Beutler et al. (2011) and the SDSS-LRG DR7-Full measurement described in Section 5 (using a binning of $10 h^{-1}$ Mpc in all cases). These correlation functions have quite different amplitudes owing to differences between the growth factors at the effective redshifts z of the samples and the bias factors b of the various galaxy tracers. Before stacking these functions we make an amplitude correction to a common redshift $z_0 = 0.35$ and bias factor $b_0 = 1$ by multiplying each correlation function by $[b_0^2 G(z_0)^2 B_0(\beta_0)]/[b^2 G(z)^2 B_0(\beta)]$ where $G(z)$ is the linear growth factor at redshift z and $B_0(\beta) = 1 + \frac{2}{3}\beta + \frac{1}{5}\beta^2$ is the Kaiser boost factor in terms of the redshift-space distortion parameter $\beta = \Omega_m(z)^{6/11}/b$ (Kaiser 1987). When calculating these quantities we assumed that the redshifts of the WiggleZ, SDSS-LRG and 6dFGS samples were $z = (0.6, 0.314, 0.106)$ and the bias factors were $b = (1.1, 2.2, 1.8)$. After making these normalization corrections we then combined the correlation functions and their corresponding covariance matrices using inverse-variance weighting in the same style as equations (12) and (13). The resulting total correlation

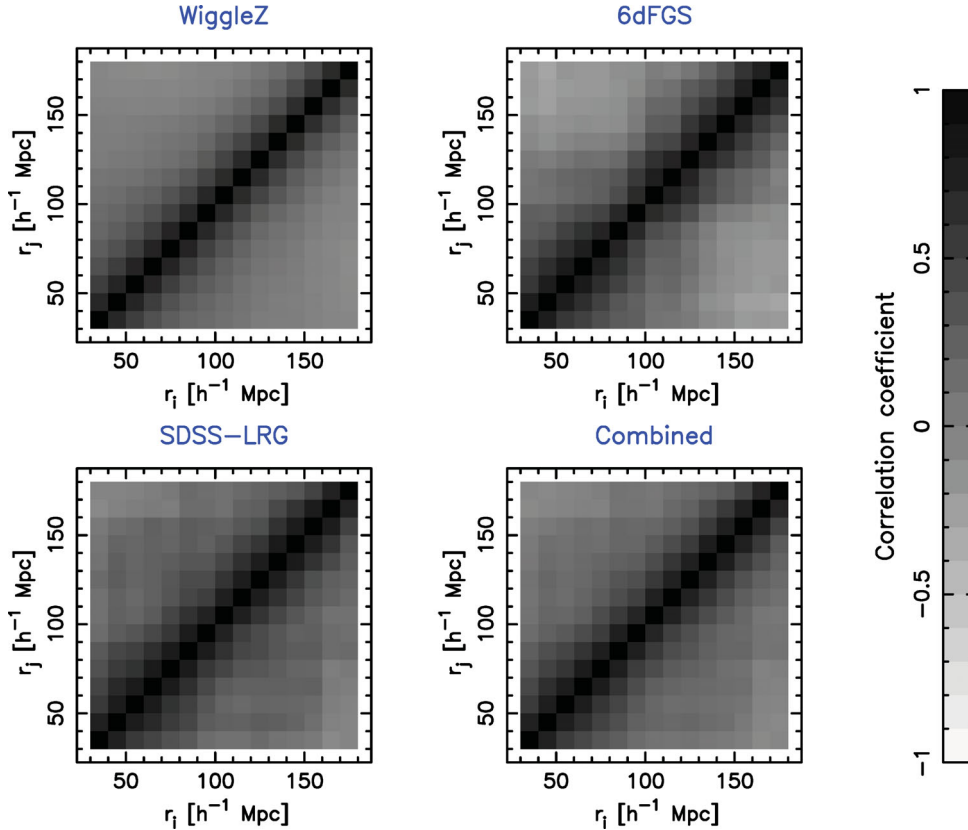


Figure 9. The amplitude of the cross-correlation $C_{ij}/\sqrt{C_{ii}C_{jj}}$ of the covariance matrix C_{ij} for the WiggleZ, SDSS-LRG and 6dFGS correlation functions. The lower-right panel shows the covariance matrix of the combined correlation function. The covariance matrices for the WiggleZ and 6dFGS samples are determined using lognormal realizations, and that of the SDSS-LRG sample is obtained from an ensemble of N -body simulations. The plot of the WiggleZ cross-correlation matrix in the upper-left panel is reproduced from the lower-right panel of Fig. 2.

function is plotted in the lower-right panel of Fig. 8. The covariance matrices of the different survey correlation functions and final combination are displayed in Fig. 9. An additional overplot of these correlation functions is provided in Fig. 10. We note that although the SDSS-LRG correlation function measurement used the fiducial cosmology $\Omega_m = 0.25$, compared to the choice $\Omega_m = 0.27$ for the WiggleZ and 6dFGS analyses, the Alcock–Paczynski distortion between these cases is negligible compared to the statistical errors in α .

6.3 Significance of the detection of the baryon acoustic peak in the combined sample

We fitted the clustering model described in Section 3 to the combined correlation function over separation range $30 < s < 180 h^{-1} \text{ Mpc}$, varying $\Omega_m h^2$, α , σ_v and b^2 and using an effective redshift $z = 0.35$. We used the more conservative minimum fitted scale $30 h^{-1} \text{ Mpc}$ for the analysis of the stacked correlation function in this section, compared to $10 h^{-1} \text{ Mpc}$ for the fits to the WiggleZ correlation function in Section 4, because (1) the required non-linear corrections become more important for galaxy samples such as the 6dFGS and SDSS LRGs, which are both more biased and at lower redshift than the WiggleZ sample, and (2) systematic errors in the fitting become relatively more important for this combined data set with higher signal-to-noise ratio. Although we fixed the relative bias factors of the galaxy samples when stacking the survey correlation functions in Section 6.2, we still marginalized over an absolute normalization $b^2 \sim 1$ when fitting the model in this section.

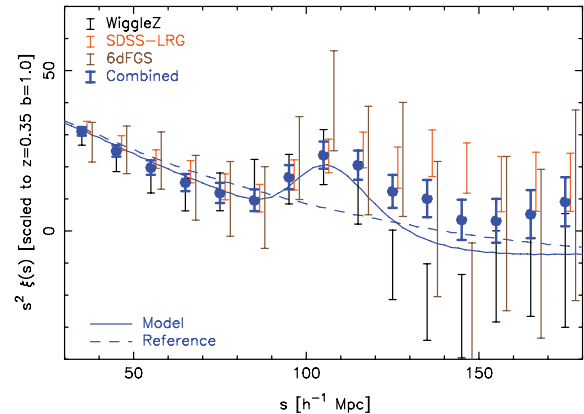


Figure 10. An overplot of the correlation function measurements $\xi(s)$ for the WiggleZ, SDSS-LRG and 6dFGS galaxy samples, plotted in the combination $s^2 \xi(s)$ where s is the comoving redshift–space separation. A normalization correction has been applied to these correlation functions to allow for the differing effective redshifts and galaxy bias factors of the samples (see the text for details). The combined correlation function, determined by inverse-variance weighting, is also plotted. The best-fitting clustering model to the combined correlation function (varying $\Omega_m h^2$, α , σ_v and b^2) is overplotted as the solid line. We also show as the dashed line the corresponding ‘no-wiggles’ reference model (Eisenstein & Hu 1998), constructed from a power spectrum with the same clustering amplitude but lacking BAOs.

We obtained a good fit to the stacked correlation function with $\chi^2 = 11.3$ (for 11 d.o.f.) and marginalized parameter values $\Omega_m h^2 = 0.132 \pm 0.014$, $\alpha = 1.037 \pm 0.036$ and $\sigma_v = 4.5 \pm 1.8 h^{-1} \text{Mpc}$. Although the best-fitting value of α must be interpreted as some effective value integrating over redshift, we can conclude that the measured BAO distance scale is consistent with the fiducial model.

We quantified the significance of the detection of the acoustic peak in the combined sample using two methods. First, we repeated the parameter fit replacing the model correlation function with one generated using a ‘no-wiggles’ reference power spectrum (Eisenstein & Hu 1998). The minimum value obtained for the χ^2 statistic in this case was 32.7, indicating that the model containing baryon oscillations was favoured by $\Delta\chi^2 = 21.4$. This corresponds to a detection of the acoustic peak with a statistical significance of 4.6σ .

As an alternative approach for assessing the significance of the detection, we changed the fiducial baryon density to $\Omega_b = 0$ and repeated the parameter fit. For zero-baryon density we generated the model matter power spectrum using the fitting formulae of Eisenstein & Hu (1998), rather than using the CAMB software. The minimum value obtained for the χ^2 statistic was now 35.3, this time suggesting that the acoustic peak had been detected with a significance of 4.9σ . The reason that the significance of detection varies between these two methods of assessment is that in the latter case, where the baryon density is changed, the overall shape of the clustering pattern is also providing information used to disfavour the $\Omega_b = 0$ model, whereas in the former case only the presence of the acoustic peak varies between the two sets of models.

7 COSMOLOGICAL PARAMETER FITS

In this section we fit cosmological models to the latest distance data sets comprising BAO, SNe and CMB measurements. Our aim is to compare parameter fits to BAO+CMB data (excluding SNe) and SNe+CMB data (excluding BAO) as a robust check for systematic errors in these distance probes.

7.1 BAO data set

The latest BAO distance data set, including the 6dFGS, SDSS and WiggleZ surveys, now comprises BAO measurements at six different redshifts. These data are summarized in Table 3. First, we use the

Table 3. The BAO distance data set from the 6dFGS, SDSS and WiggleZ surveys. Measurements of the distilled parameters d_z and $A(z)$ are quoted. The most appropriate choices to be used in cosmological parameter fits are indicated by bold font. For the SDSS data, the values of $A(z)$ are obtained by scaling from the measurements of d_z reported by Percival et al. (2010) using their fiducial cosmological parameters and the same fractional error. The pairs of measurements at $z = (0.2, 0.35)$, $z = (0.44, 0.6)$ and $z = (0.6, 0.73)$ are correlated with coefficients 0.337, 0.369 and 0.438, respectively. The inverse covariance matrix of the data points at $z = (0.2, 0.35)$ is given by equation (5) in Percival et al. (2010). The inverse covariance matrix of the data points at $z = (0.44, 0.6, 0.73)$ is given in Table 2. The other measurements are uncorrelated.

Sample	z	d_z	$A(z)$
6dFGS	0.106	0.336 ± 0.015	0.526 ± 0.028
SDSS	0.2	0.1905 ± 0.0061	0.488 ± 0.016
SDSS	0.35	0.1097 ± 0.0036	0.484 ± 0.016
WiggleZ	0.44	0.0916 ± 0.0071	0.474 ± 0.034
WiggleZ	0.6	0.0726 ± 0.0034	0.442 ± 0.020
WiggleZ	0.73	0.0592 ± 0.0032	0.424 ± 0.021

measurement of $d_{0.106} = 0.336 \pm 0.015$ from the 6dFGS reported by Beutler et al. (2011). Secondly, we add the two correlated measurements of $d_{0.2}$ and $d_{0.35}$ determined by Percival et al. (2010) from fits to the power spectra of LRGs and main-sample galaxies in the SDSS (spanning a range of wavenumbers $0.02 < k < 0.3 h \text{Mpc}^{-1}$). The correlation coefficient for these last two measurements is 0.337. We note that our own LRG baryon acoustic peak measurements reported in Section 5 are entirely consistent with these fits. Finally, we include the three correlated measurements of $A(z = 0.44)$, $A(z = 0.6)$ and $A(z = 0.73)$ reported in this study, using the inverse covariance matrix listed in Table 2.

In our cosmological model fitting we assume that the BAO distance errors are Gaussian in nature. Modelling potential non-Gaussian tails in the likelihood is beyond the scope of this paper, although we note that they may not be negligible (Percival et al. 2007, 2010; Bassett & Afshordi 2010). We caution that the 2σ confidence regions displayed in the figures in this section might not necessarily follow the Gaussian scaling. The WiggleZ and SDSS-LRG surveys share a sky overlap of $\approx 500 \text{deg}^2$ for redshift range $z < 0.5$; given that the SDSS-LRG measurement is derived across a sky area $\approx 8000 \text{deg}^2$ and the errors in both measurements contain a significant component due to shot noise, the resulting covariance is negligible.

This BAO distance data set is plotted in Fig. 11 relative to a flat Λ CDM cosmological model with matter density $\Omega_m = 0.29$ and Hubble parameter $h = 0.69$ (these values provide the best fit to the combined cosmological data sets as discussed below). The panels of Fig. 11 show various representations of the BAO data set including $D_V(z)$ and the distilled parameters $A(z)$ and d_z .

7.2 SNe data set

We used the ‘Union 2’ compilation by Amanullah et al. (2010) as our supernova data set, obtained from the website <http://supernova.lbl.gov/Union>. This compilation of 557 SNe includes data from Hamuy et al. (1996), Riess et al. (1999, 2007), Astier et al. (2006), Jha et al. (2006), Wood-Vasey et al. (2007), Holtzman et al. (2008), Hicken et al. (2009) and Kessler et al. (2009). The data are represented as a set of values of the distance modulus for each supernova

$$\mu = 5 \log_{10} \left[\frac{D_L(z)}{1 \text{Mpc}} \right] + 25, \quad (15)$$

where $D_L(z)$ is the luminosity distance at redshift z . The values of μ are reported for a particular choice of the normalization $M - 5 \log_{10} h$, which is marginalized as an unknown parameter in our analysis as described below. When fitting cosmological models to these SNe data we used the full covariance matrix of these measurements including systematic errors, as reported by Amanullah et al. (2010).

Fig. 12 is a representation of the consistency and relative accuracy with which baryon oscillation measurements and SNe currently map out the cosmic distance scale. In order to construct this figure we converted the BAO measurements of $D_V(z)$ into $D_A(z)$ assuming a Hubble parameter $H(z)$ for a flat Λ CDM model with $\Omega_m = 0.29$ and $h = 0.69$. The binned SNe data currently measure the distance–redshift relation at $z < 0.8$ with three to four times higher accuracy than the BAOs, although we note that the consequences for cosmological parameter fits are highly influenced by the differing normalization of the two methods. The SNe measure the relative luminosity distance to the relation at $z = 0$, $D_L(z)H_0/c$,

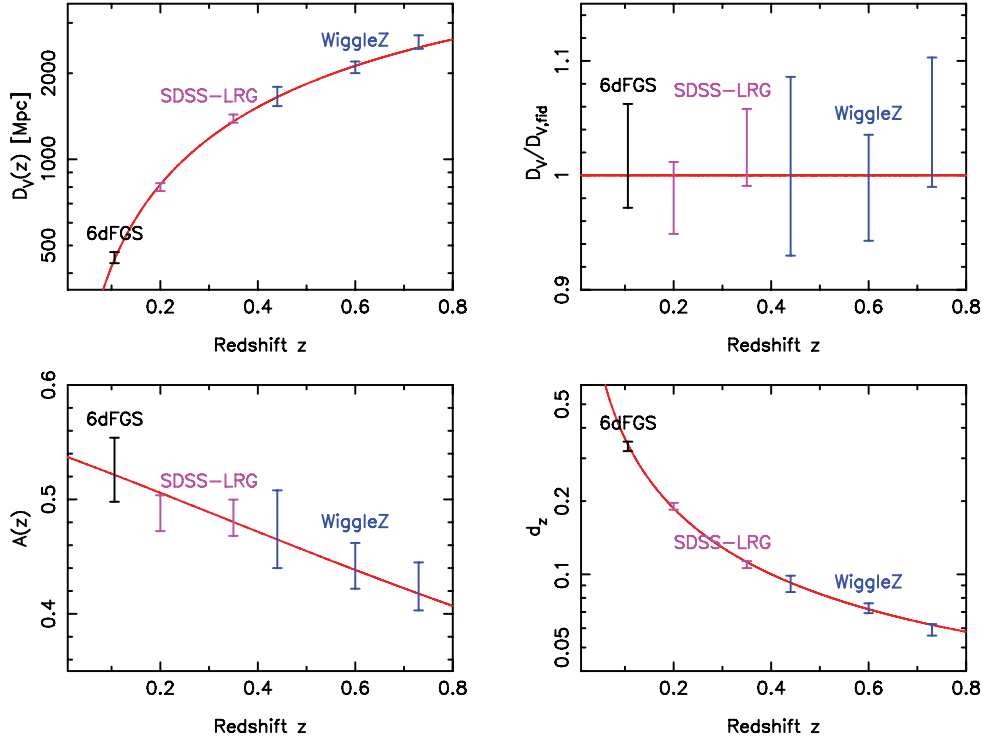


Figure 11. Current measurements of the cosmic distance scale using the BAO standard ruler applied to the 6dFGS, SDSS and WiggleZ surveys (where the data are taken from Percival et al. 2010; Beutler et al. 2011 and this study). The results are compared to a flat Λ CDM cosmological model with matter density $\Omega_m = 0.29$ and Hubble parameter $h = 0.69$. Various representations of the data are shown: the BAO distance $D_V(z)$ recovered from fits to the angle-averaged clustering measurements (top-left panel); these distances ratioed to the fiducial model (top-right panel), the distilled parameter $A(z)$ (defined by equation 14) extracted from fits governed by both the acoustic peak and clustering shape (bottom-left panel), and the distilled parameter d_z determined by fits controlled by solely the acoustic peak information (bottom-right panel). We note that the conversion of the BAO fits to the measurements of $D_V(z)$ presented in the upper two plots requires a value for the standard ruler scale to be assumed: we take $r_s(z_d) = 152.40$ Mpc, obtained using equation (6) in Eisenstein & Hu (1998) evaluated for our fiducial model $\Omega_m h^2 = 0.1381$ and $\Omega_b h^2 = 0.02227$.

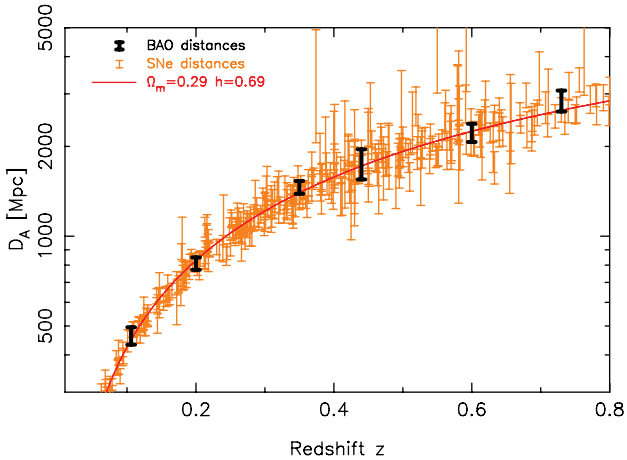


Figure 12. Comparison of the accuracy with which SNe and BAOs map out the cosmic distance scale at $z < 0.8$. For the purposes of this figure, BAO measurements of $D_V(z)$ have been converted into $D_A(z)$ assuming a Hubble parameter $H(z)$ for a flat Λ CDM model with $\Omega_m = 0.29$ and $h = 0.69$, indicated by the solid line in the figure, and SNe measurements of $D_L(z)$ have been plotted assuming $D_A(z) = D_L(z)/(1+z)^2$.

owing to the unknown value of the standard candle absolute magnitude M . The BAOs measure a distance scale relative to the sound horizon at baryon drag calibrated by the CMB data, effectively an absolute measurement of $D_V(z)$ given that the error is dominated

by the statistical uncertainty in the clustering fits, rather than any systematic uncertainty in the sound horizon calibration from the CMB.

When undertaking cosmological fits to the SNe data set, we performed an analytic marginalization over the unknown absolute normalization $M - 5 \log_{10} h$ (Goliath et al. 2001; Bridle et al. 2002). This is carried out by determining the chi-squared statistic for each cosmological model as

$$\chi^2 = \mathbf{y}^T \mathbf{C}_{\text{SN}}^{-1} \mathbf{y} - \frac{\left(\sum_{ij} C_{\text{SN},ij}^{-1} y_j \right)^2}{\sum_{ij} C_{\text{SN},ij}^{-1}} \quad (16)$$

where \mathbf{y} is the vector representing the difference between the distance moduli of the data and model, and $\mathbf{C}_{\text{SN}}^{-1}$ is the inverse covariance matrix for the SNe distance moduli.

7.3 CMB data set

We included the CMB data in our cosmological fits using the *WMAP* ‘distance priors’ (Komatsu et al. 2009) using the 7-year *WMAP* results reported by Komatsu et al. (2011). The distance priors quantify the complete CMB likelihood via a three-parameter covariance matrix for the acoustic index ℓ_A , the shift parameter \mathcal{R} and the redshift of recombination z_* , as given in table 10 of Komatsu et al. (2011). When deriving these quantities we assumed a physical baryon density $\Omega_b h^2 = 0.02227$, a CMB temperature $T_{\text{CMB}} = 2.725$ K and a number of relativistic degrees of freedom $N_{\text{eff}} = 3.04$.

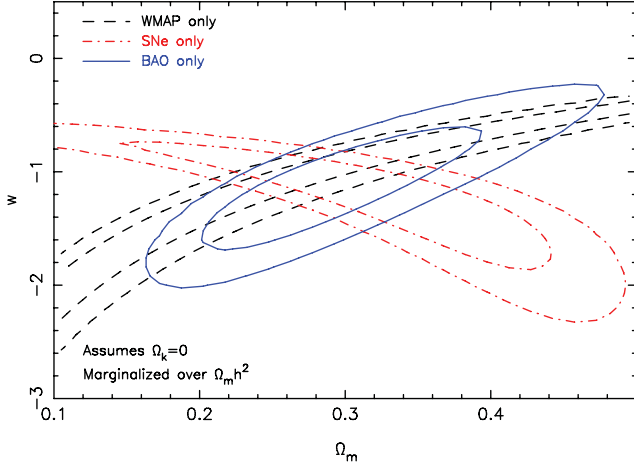


Figure 13. The joint probability for parameters Ω_m and w fitted separately to the *WMAP*, BAO and SNe distance data, marginalized over $\Omega_m h^2$ and assuming $\Omega_k = 0$. The two contour levels in each case enclose regions containing 68.27 per cent and 95.45 per cent of the total likelihood.

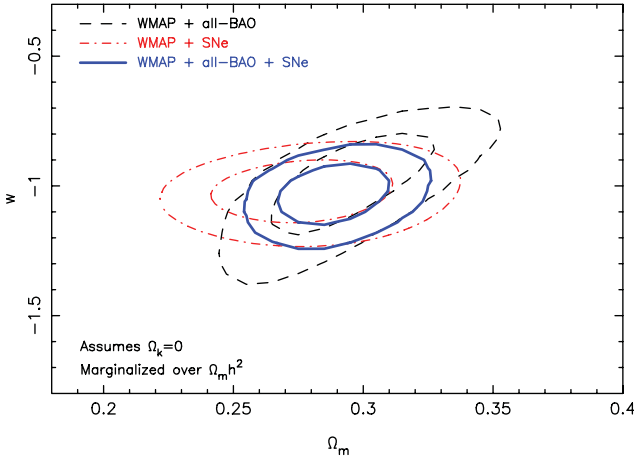


Figure 14. The joint probability for parameters Ω_m and w fitted to various combinations of *WMAP*, BAO and SNe distance data, marginalized over $\Omega_m h^2$ and assuming $\Omega_k = 0$. The two contour levels in each case enclose regions containing 68.27 per cent and 95.45 per cent of the total likelihood.

7.4 Flat w models

We first fitted a flat w CDM cosmological model in which spatial curvature is fixed at $\Omega_k = 0$ but the equation-of-state w of dark energy is varied as a free parameter. We fitted for the three parameters (Ω_m , $\Omega_m h^2$, w) using flat, wide priors which extend well beyond the regions of high likelihood and have no effect on the cosmo-

logical fits. The best-fitting model has $\chi^2 = 532.9$ for 563 d.o.f., representing a good fit to the distance data set.

Figs 13 and 14 compare the joint probability of Ω_m and w , marginalizing over $\Omega_m h^2$, for the individual *WMAP*, BAO and SNe data sets along with various combinations. We note that for the ‘BAO only’ contours in Fig. 13, we have not used any CMB calibration of the standard ruler scale $r_s(z_d)$, and thus the 6dFGS and SDSS measurements of $d_z = r_s(z_d)/D_V(z)$ do not contribute strongly to these constraints. Hence, the addition of the CMB data in Fig. 14 has the benefit of both improving the information from the d_z measurements by determining $r_s(z_d)$ and contributing the *WMAP* distance prior constraints. The *WMAP*+BAO and *WMAP*+SNe data produce consistent determinations of the cosmological parameters, with the error in the equation-of-state $\Delta w \approx 0.1$. Combining all three data sets produces the marginalized result $w = -1.034 \pm 0.080$ (errors in the other parameters are listed in Table 4; the quoted error in h results from fitting the three parameters Ω_m , h and w). The best-fitting equation-of-state is consistent with a cosmological constant model for which $w = -1$.

We caution that the probability contours plotted in Figs 13 and 14 (and other similar figures in this section) assume that the errors in the BAO distance data set are Gaussian. If the likelihood contains a significant non-Gaussian tail, the 2σ region could be affected.

We repeated the *WMAP*+BAO fit comparing the two different implementations of the SDSS-LRG BAO distance-scale measurements: the Percival et al. (2010) power spectrum fitting at $z = 0.2$ and $z = 0.35$, and our correlation function fit presented in Section 5. We found that the marginalized measurements of w in the two cases were -1.00 ± 0.13 and -0.97 ± 0.13 , respectively. Our results are therefore not significantly changed by the methodology used for these LRG fits.

7.5 Curved Λ models

We next fitted a curved Λ CDM model, in which we fixed the equation-of-state of dark energy at $w = -1$ but added the spatial curvature Ω_k as an additional free parameter. We fitted for the three parameters (Ω_m , $\Omega_m h^2$, Ω_k) using flat, wide priors which extend well beyond the regions of high likelihood and have no effect on the cosmological fits. The best-fitting model has $\chi^2 = 532.7$ for 563 d.o.f.

Figs 15 and 16 compare the joint probability of Ω_m and Ω_k , marginalizing over $\Omega_m h^2$, for the individual *WMAP*, BAO and SNe data sets along with various combinations. Once more, we find that fits to *WMAP*+BAO and *WMAP*+SNe produce mutually consistent results. The BAO data have higher sensitivity to curvature because of the long lever arm represented by the relation of distance measurements at $z < 1$ and at recombination. Combining all three data sets produces the marginalized result $\Omega_k = -0.0040 \pm 0.0062$ (errors in the other parameters are listed in

Table 4. The results of fitting various cosmological models to a combination of the latest CMB, BAO and SNe distance data sets. Measurements and 1σ errors are listed for each parameter, marginalizing over the other parameters of the model. All models contain either $(\Omega_m, \Omega_m h^2)$ or (Ω_m, h) amongst the parameters fitted.

Model	χ^2	d.o.f.	Ω_m	$\Omega_m h^2$	h	Ω_k	w_0	w_a
Flat Λ CDM	533.1	564	0.290 ± 0.014	0.1382 ± 0.0029	0.690 ± 0.009	–	–	–
Flat w CDM	532.9	563	0.289 ± 0.015	0.1395 ± 0.0043	0.696 ± 0.017	–	-1.034 ± 0.080	–
Curved Λ CDM	532.7	563	0.292 ± 0.014	0.1354 ± 0.0054	0.681 ± 0.017	-0.0040 ± 0.0062	–	–
Curved w CDM	531.9	562	0.289 ± 0.015	0.1361 ± 0.0055	0.687 ± 0.019	-0.0061 ± 0.0070	-1.063 ± 0.094	–
Flat $w(a)$ CDM	531.9	562	0.288 ± 0.016	0.1386 ± 0.0053	0.695 ± 0.017	–	-1.094 ± 0.171	0.194 ± 0.687

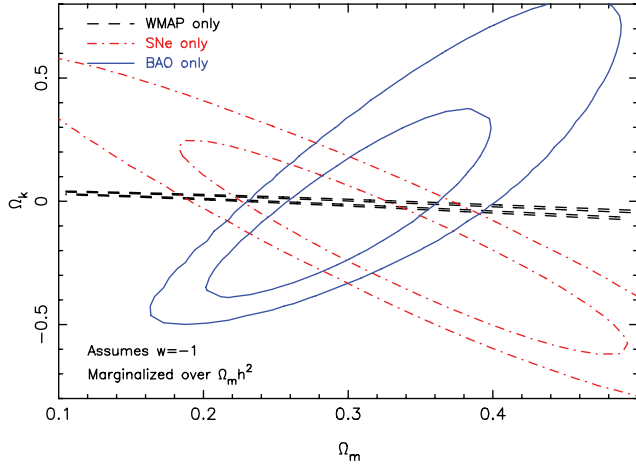


Figure 15. The joint probability for parameters Ω_m and Ω_k fitted separately to the *WMAP*, BAO and SNe distance data, marginalized over $\Omega_m h^2$ and assuming $w = -1$. The two contour levels in each case enclose regions containing 68.27 per cent and 95.45 per cent of the total likelihood.

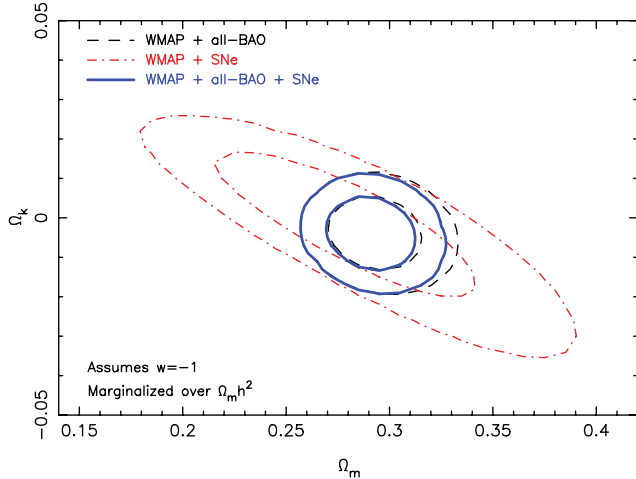


Figure 16. The joint probability for parameters Ω_m and Ω_k fitted to various combinations of *WMAP*, BAO and SNe distance data, marginalized over $\Omega_m h^2$ and assuming $w = -1$. The two contour levels in each case enclose regions containing 68.27 per cent and 95.45 per cent of the total likelihood.

Table 4). The best-fitting parameters are consistent with zero spatial curvature.

7.6 Additional degrees of freedom

We fitted two further cosmological models, each containing an additional parameter. First we fitted a curved w CDM model in which we varied both the dark energy equation-of-state and the spatial curvature as free parameters. The best-fitting model has $\chi^2 = 531.9$ for 562 d.o.f., representing an improvement of $\Delta\chi^2 = 1.0$ compared to the case where $\Omega_k = 0$, for the addition of a single extra parameter. In terms of information criteria this does not represent a sufficient improvement to justify the addition of the extra degree of freedom. Fig. 17 compares the joint probability of w and Ω_k , marginalizing over Ω_m and $\Omega_m h^2$, for the three cases *WMAP*+BAO, *WMAP*+SNe and *WMAP*+BAO+SNe. Combining all three data sets produces the marginalized measurements $w = -1.063 \pm 0.094$ and $\Omega_k = -0.0061 \pm 0.0070$.

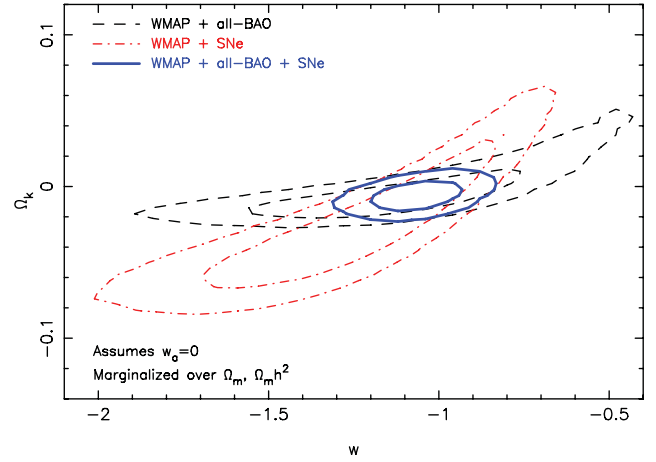


Figure 17. The joint probability for parameters Ω_k and w fitted to various combinations of *WMAP*, BAO and SNe distance data, marginalized over Ω_m and $\Omega_m h^2$. The two contour levels in each case enclose regions containing 68.27 per cent and 95.45 per cent of the total likelihood.

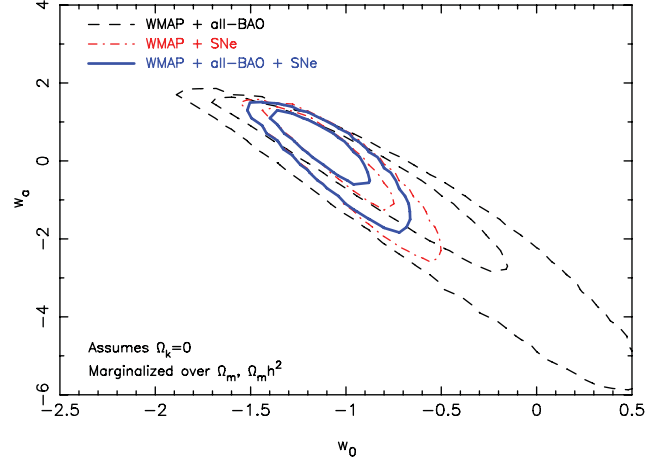


Figure 18. The joint probability for parameters w_0 and w_a describing an evolving equation-of-state for dark energy, fitted to various combinations of *WMAP*, BAO and SNe distance data, marginalized over Ω_m and $\Omega_m h^2$ and assuming $\Omega_k = 0$. The two contour levels in each case enclose regions containing 68.27 per cent and 95.45 per cent of the total likelihood.

We finally fitted a flat $w(a)$ CDM cosmological model in which spatial curvature is fixed at $\Omega_k = 0$ but the equation-of-state of dark energy is allowed to vary with scalefactor a in accordance with the Chevallier–Polarski–Linder parametrization $w(a) = w_0 + (1 - a)w_a$ (Chevallier & Polarski 2001; Linder 2003). The best-fitting model has $\chi^2 = 531.9$ for 562 d.o.f., and again the improvement in the value of χ^2 compared to the case where $w_a = 0$ does not justify the addition of the extra degree of freedom. Fig. 18 compares the joint probability of w_0 and w_a , marginalizing over Ω_m and $\Omega_m h^2$, in the same style as Fig. 17. Combining all three data sets produces the marginalized measurements $w_0 = -1.09 \pm 0.17$ and $w_a = 0.19 \pm 0.69$. We note that the addition of the BAO measurements to the *WMAP*+SNe data set produces a more significant improvement for fits involving Ω_k than for w_a .

In all cases, the best-fitting parameters are consistent with a flat cosmological constant model for which $w_0 = -1$, $w_a = 0$ and $\Omega_k = 0$. The best-fitting values and errors in the parameters for the various models, for the fits using all three data sets, are listed in Table 4.

8 CONCLUSIONS

We summarize the results of our study as follows.

(i) The final data set of the WiggleZ Dark Energy Survey allows the imprint of the baryon acoustic peak to be detected in the galaxy correlation function for independent redshift slices of width $\Delta z = 0.4$. A simple quasi-linear acoustic peak model provides a good fit to the correlation functions over a range of separations $10 < s < 180 h^{-1}$ Mpc. The resulting distance-scale measurements are determined by both the acoustic peak position and the overall shape of the clustering pattern, such that the whole correlation function is being used as a standard ruler. As such, the acoustic parameter $A(z)$ introduced by Eisenstein et al. (2005) represents the most appropriate distilled parameter for quantifying the WiggleZ BAO measurements, and we present in Table 2 a 3×3 covariance matrix describing the determination of $A(z)$ from WiggleZ data at the three redshifts $z = 0.44, 0.6$ and 0.73 . We test for systematics in this measurement by varying the fitting range and implementation of the quasi-linear model, and also by repeating our fits for a dark matter halo subset of the GiggleZ simulation. In no case do we find evidence for significant systematic error.

(ii) We present a new measurement of the baryon acoustic feature in the correlation function of the SDSS-LRG sample, finding that the feature is detected within a subset spanning the redshift range $0.16 < z < 0.44$ with a statistical significance of 3.4σ . We derive a measurement of the distilled parameter $d_z = 0.314 = 0.1239 \pm 0.0033$ that is consistent with previous analyses of the LRG power spectrum.

(iii) We combine the galaxy correlation functions measured from the WiggleZ, 6dFGS and SDSS-LRG samples. Each of these data sets shows independent evidence for the baryon acoustic peak, and the combined correlation function contains a BAO detection with a statistical significance of 4.9σ relative to a zero-baryon model with no peak.

(iv) We fit cosmological models to the combined 6dFGS, SDSS and WiggleZ BAO data set, now comprising six distance–redshift data points, and compare the results to similar fits to the latest compilation of SNe and CMB data. The BAO and SNe data sets produce consistent measurements of the equation-of-state w of dark energy, when separately combined with the CMB, providing a powerful check for systematic errors in either of these distance probes. Combining all data sets, we determine $w = -1.034 \pm 0.080$ for a flat universe, and $\Omega_k = -0.0040 \pm 0.0062$ for a curved, cosmological-constant universe.

(v) Adding extra degrees of freedom always produces best-fitting parameters consistent with a cosmological constant dark-energy model within a spatially flat universe. Varying both curvature and w , we find marginalized errors $w = -1.063 \pm 0.094$ and $\Omega_k = -0.0061 \pm 0.0070$. For a dark-energy model evolving with scale-factor a such that $w(a) = w_0 + (1 - a)w_a$, we find that $w_0 = -1.09 \pm 0.17$ and $w_a = 0.19 \pm 0.69$.

In conclusion, we have presented and analysed the most comprehensive BAO data set assembled to date. Results from the WiggleZ Dark Energy Survey have allowed us to extend this data set up to redshift $z = 0.73$, thereby spanning the whole redshift range for which dark energy is hypothesized to govern the cosmic expansion history. By fitting cosmological models to this data set we have established that a flat Λ CDM cosmological model continues to provide a good and self-consistent description of CMB, BAO and SNe data. In particular, the BAO and SNe yield consistent measurements

of the distance–redshift relation across the common redshift interval probed. Our results serve as a baseline for the analysis of future CMB data sets provided by the *Planck* satellite (Ade et al. 2011) and BAO measurements from the Baryon Oscillation Spectroscopic Survey (Eisenstein et al. 2011).

ACKNOWLEDGMENTS

We thank the anonymous referee for careful and constructive comments that improved this study.

We acknowledge financial support from the Australian Research Council through Discovery Project grants DP0772084 and DP1093738 funding the positions of SB, DP, MP, GP and TMD. SC and DC acknowledge the support of the Australian Research Council through QEII Fellowships. MJD thanks the Gregg Thompson Dark Energy Travel Fund for financial support.

We thank the LasDamas project for making their mock catalogues publicly available. In particular EK is much obliged to Cameron McBride for supplying mock catalogues on demand. EK also thanks Ariel Sánchez for fruitful lengthy discussions. EK was partially supported by a Google Research Award and NASA Award.

FB is supported by the Australian Government through the International Postgraduate Research Scholarship (IPRS) and by scholarships from the International Centre for Radio Astronomy Research (ICRAR) and the Australian Astronomical Observatory (AAO).

GALEX is a NASA Small Explorer, launched in 2003 April. We gratefully acknowledge NASA’s support for construction, operation and science analysis for the *GALEX* mission, developed in cooperation with the Centre National d’Etudes Spatiales of France and the Korean Ministry of Science and Technology.

Finally, the WiggleZ survey would not be possible without the dedicated work of the staff of the Australian Astronomical Observatory in the development and support of the AAOmega spectrograph, and the running of the Anglo-Australian Telescope (AAT).

REFERENCES

- Ade P. et al., 2011, A&A, in press (arXiv:1101.2022)
Amanullah R. et al., 2010, ApJ, 716, 712
Astier P. et al., 2006, A&A, 447, 31
Bardeen J. M., Bond J. R., Kaiser N., Szalay A. S., 1986, ApJ, 304, 15
Bassett B., Afshordi N., 2010, preprint (arXiv:1005.1664)
Berlind A. A., Weinberg D. H., 2002, ApJ, 575, 587
Beutler F. et al., 2011, MNRAS, in press (arXiv:1106.3366)
Blake C. A., Glazebrook K., 2003, ApJ, 594, 665
Blake C. A., Parkinson D., Bassett B., Glazebrook K., Kunz M., Nichol R. C., 2006, MNRAS, 365, 255
Blake C. A., Collister A., Bridle S., Lahav O., 2007, MNRAS, 374, 1527
Blake C. et al., 2010, MNRAS, 406, 803
Blake C. et al., 2011, MNRAS, 415, 2892
Blanton M., Lin H., Lupton R., Maley F. M., Young N., Zehavi I., Loveday J., 2003, AJ, 125, 2276
Bond J. R., Efstathiou G., 1984, ApJ, 285, L45
Bridle S. L., Crittenden R., Melchiorri A., Hobson M. P., Kneissl R., Lasenby A. N., 2002, MNRAS, 335, 1193
Cabre A., Gaztanaga E., 2011, MNRAS, 412, 98
Chevallier M., Polarski D., 2001, Int. J. Mod. Phys., D10, 213
Cole S. et al., 2005, MNRAS, 362, 505
Cooray A., Hu W., Huterer D., Joffe M., 2001, ApJ, 557, L7
Copin Y. et al., 2006, New Astron. Rev., 50, 436
Croce M., Scoccimarro R., 2008, Phys. Rev. D, 2008, 77, 3533
Croce M., Gaztanaga E., Cabre A., Carnero E., Sánchez E., 2011, MNRAS, in press (arXiv:1104.5236)

- Dawson K. S. et al., 2009, *AJ*, 138, 1271
 Drinkwater M. et al., 2010, *MNRAS*, 401, 1429
 Efstathiou G., Sutherland W., Maddox S., 1990, *Nat*, 348, 705
 Eisenstein D. J., 2003, in Brown M., Dey A., eds, *ASP Conf. Series Vol. 280, Large-scale Structure and Future Surveys. Next Generation Wide Field Multi-Object Spectroscopy*. Astron. Soc. Pac., San Francisco, preprint (astro-ph/0301623)
 Eisenstein D. J., Hu W., 1998, *ApJ*, 496, 605
 Eisenstein D. J., Hu W., Tegmark M., 1998, *ApJ*, 504, 57
 Eisenstein D. J. et al., 2001, *AJ*, 122, 2267
 Eisenstein D. J. et al., 2005, *ApJ*, 633, 560
 Eisenstein D. J., Seo H.-J., White M., 2007, *ApJ*, 664, 660
 Eisenstein D. J. et al., 2011, *AJ*, 142, 72
 Fukugita M., Ichikawa T., Gunn J. E., Doi M., Shimasaku K., Schneider D. P., 1996, *AJ*, 111, 1748
 Gilbank D. G., Gladders M. G., Yee H. K. C., Hsieh B. C., 2011, *AJ*, 141, 94
 Glazebrook K., Blake C. A., 2005, *ApJ*, 631, 1
 Goliath M., Amanullah R., Astier P., Goobar A., Pain R., 2001, *A&A*, 380, 6
 Gunn J. E. et al., 1998, *AJ*, 116, 3040
 Gunn J. E. et al., 2006, *AJ*, 131, 2332
 Hamuy M. et al., 1996, *AJ*, 112, 2408
 Hamuy M. et al., 2006, *PASP*, 118, 2
 Hicken M. et al., 2009, *ApJ*, 700, 331
 Hogg D. W., Finkbeiner D. P., Schlegel D. J., Gunn J. E., 2001, *AJ*, 122, 2129
 Holtzman J. A., 1989, *ApJS*, 71, 1
 Holtzman J. A. et al., 2008, *AJ*, 136, 2306
 Hu W., Haiman Z., 2003, *Phys. Rev. D.*, 68, 063004
 Hu W., Sugiyama N., 1996, *ApJ*, 471, 542
 Hutsi G., 2006, *A&A*, 449, 891
 Ivezić Z. et al., 2004, *Astron. Nachr.*, 325, 583
 Jarrett T., Chester T., Cutri R., Schneider S., Strutskie M., Huchra J. P., 2000, *AJ*, 119, 2498
 Jha S. et al., 2006, *AJ*, 131, 527
 Jones D. H. et al., 2009, *MNRAS*, 399, 683
 Kaiser N., 1987, *MNRAS*, 227, 1
 Kazin E. A. et al., 2010a, *ApJ*, 710, 1444
 Kazin E. A., Blanton M. R., Scoccimarro R., McBride C. K., Berlind A. A., 2010b, *ApJ*, 719, 1032
 Kazin E. A., Sánchez A. G., Blanton M. R., 2011, *MNRAS*, submitted (arXiv:1105.2037)
 Kessler R. et al., 2009, *ApJS*, 185, 32
 Komatsu E. et al., 2009, *ApJS*, 180, 330
 Komatsu E. et al., 2011, *ApJS*, 192, 18
 Kowalski M. et al., 2008, *ApJ*, 686, 749
 Krauss L. M., Turner M. S., 1995, *Gen. Relativity Grav.*, 27, 1137
 Landy S. D., Szalay A. S., 1993, *ApJ*, 412, 64
 Law N. et al., 2009, *PASP*, 121, 1395
 Lewis A., Challinor A., Lasenby A., 2000, *ApJ*, 538, 473
 Linder E. V., 2003, *Phys. Rev. Lett.*, 90, 091301
 Lupton R., Gunn J. E., Ivezić Z., Knapp G. R., Kent S., 2001, in Hamden F. R., Jr, Primiini F. A., Payne H. E., eds, *ASP Conf. Ser. Vol. 238, Astronomical Data Analysis Software and Systems X*, Astron. Soc. Pac., San Francisco, p. 269
 Martin D. et al., 2005, *ApJ*, 619, L1
 Matsubara T., 2008, *Phys. Rev. D.*, 78, 083519
 Miller C. J., Nichol R. C., Batuski D. J., 2001, *ApJ*, 555, 68
 Ostriker J., Steinhardt P., 1995, *Nat*, 377, 600
 Padmanabhan N., White M., 2008, *Phys. Rev. D.*, 77, 3540
 Padmanabhan N., White M., 2009, *Phys. Rev. D.*, 80, 63508
 Padmanabhan N. et al., 2007, *MNRAS*, 378, 852
 Peebles P. J. E., Yu J. T., 1970, *ApJ*, 162, 815
 Percival W. J. et al., 2001, *MNRAS*, 327, 1297
 Percival W. J. et al., 2007, *ApJ*, 657, 51
 Percival W. J. et al., 2010, *MNRAS*, 401, 2148
 Perlmutter S. et al., 1999, *ApJ*, 517, 565
 Pier J. R., Munn J. A., Hindsley R. B., Hennessy G. S., Kent S. M., Lupton R. H., Ivezić Z., 2003, *AJ*, 125, 1559
 Richards G. et al., 2002, *AJ*, 123, 2945
 Riess A. G. et al., 1998, *AJ*, 116, 1009
 Riess A. G. et al., 1999, *AJ*, 117, 707
 Riess A. G. et al., 2004, *ApJ*, 607, 665
 Riess A. G. et al., 2007, *ApJ*, 659, 98
 Rimes C. D., Hamilton A. J. S., 2005, *MNRAS*, 360, 82
 Ross A. et al., 2011, *MNRAS*, submitted (arXiv:1105.2320)
 Sánchez A. G., Baugh C. M., Angulo R., 2008, *MNRAS*, 390, 1470
 Sánchez A. G., Crocce M., Cabre A., Baugh C. M., Gaztanaga E., 2009, *MNRAS*, 400, 1643
 Saunders W. et al., 2004, in Moorwood A. F. M., Masanori I., eds, *Proc. SPIE Vol. 5492, Ground-based Instrumentation for Astronomy*. SPIE, Bellingham, p. 389
 Seo H.-J., Eisenstein D. J., 2003, *ApJ*, 598, 720
 Seo H.-J., Siegel E. R., Eisenstein D. J., White M., 2008, *ApJ*, 686, 13
 Sharp R. et al., 2006, in McLean I. S., Masanori I., eds, *Proc. SPIE Vol. 6269, Ground-based and Airborne Instrumentation for Astronomy*. SPIE, Bellingham, p. 14
 Shoji M., Jeong D., Komatsu E., 2009, *ApJ*, 693, 1404
 Smith J. A. et al., 2002, *AJ*, 123, 2121
 Smith R. E. et al., 2003, *MNRAS*, 341, 1311
 Smith R. E., Scoccimarro R., Sheth R., 2008, *Phys. Rev. D.*, 77, 43525
 Stoughton C. et al., 2002, *AJ*, 123, 485
 Strauss M. et al., 2002, *AJ*, 124, 1810
 Sunyaev R. A., Zeldovitch Y. B., 1970, *Ap&SS*, 7, 3
 Takahashi R. et al., 2011, *ApJ*, 726, 7
 Taruya A., Nishimichi T., Saito S., 2010, *Phys. Rev. D.*, 82, 3522
 Tegmark M., 1997, *Phys. Rev. Lett.*, 79, 20
 Thomas S., Abdalla F., Lahav O., 2011, *Phys. Rev. Lett.*, 106, 1301
 Tucker D. L. et al., 2006, *Astron. Nachr.*, 327, 821
 White M. et al., 2011, *ApJ*, 728, 126
 Wood-Vasey W. M. et al., 2007, *ApJ*, 666, 694
 York D. G. et al., 2000, *AJ*, 120, 1579

This paper has been typeset from a $\text{\TeX}/\text{\LaTeX}$ file prepared by the author.